soluble interleukin-2 receptors in patients with HTLV-I-associated myelopathy. Am J Trop Med Hyg 42:365–373

McGill NK, Vyas J, Shimauchi T, Tokura Y, Piguet V (2012) HTLV-1-associated infective dermatitis: updates on the pathogenesis. Exp Dermatol 21:815–821

Misu T, Onodera H, Fujihara K, Matsushima K, Yoshie O, Okita N, Takase S, Itoyama Y (2001) Chemokine receptor expression on T cells in blood and cerebrospinal fluid at relapse and remission of multiple sclerosis: imbalance of Th1/Th2-associated chemokine signaling. J Neuroimmunol 114:207–212

Mitsuhiro O (1990) Review of WHO kagoshima meeting and diagnostic guidelines for HAM/TSP. Raven Press, New York, pp 191–197

Mochizuki M, Watanabe T, Yamaguchi K, Yoshimura K, Nakashima S, Shirao M, Araki S, Takatsuki K, Mori S, Miyata N (1992) Uveitis associated with human T-cell lymphotropic virus type I. Am J Ophthalmol 114:123–129

Natsumi A, Tomoo S, Hitoshi A, Yoshihisa Y (2014) HTLV-1 induces a Th1-like state in CD4+CCR4+ T cells. J Clin Invest 124:3431–3442

Niederwieser D, Huber C, Gratwohl A, Bannert P, Fuchs D, Hausen A, Reibnegger D, Speck B, Wachter H (1984) Neopterin as a new biochemical marker in the clinical monitoring of bone marrow transplant recipients. Transplantation 38:497–500

Ohba N, Matsumoto M, Sameshima M, Kabayama Y, Nakao K, Unoki K, Uehara F, Kawano K, Maruyama I, Osame M (1989) Ocular manifestations in patients infected with human T-lymphotropic virus type I. Jpn J Ophthalmol 33:1–12

Osame M, Usuku K, Izumo S, Ijichi N, Amitani H, Igata A, Matsumoto M, Tara M (1986) HTLV-I associated myelopathy, a new clinical entity. Lancet 1:1031–1032

Poiesz BJ, Ruscetti FW, Gazdar AF, Bunn PA, Minna JD, Gallo RC (1980) Detection and isolation of type C retrovirus particles from fresh and cultured lymphocytes of a patient with cutaneous T-cell lymphoma. Proc Natl Acad Sci U S A 77:7415–7419

Sato T, Coler-Reilly A, Utsunomiya A, Araya N, Yagishita N, Ando H, Yamauchi J, Inoue E, Ueno T, Hasegawa Y, Nishioka K, Nagajima T, Jacobson S, Izumo S, Yamano Y (2013) CSF CXCL10, CXCL9, and neopterin as candidate prognostic biomarkers for HTLV-1-associated myelopathy/tropical spastic paraparesis. PLoS Negl Trop Dis 7:e2479

Shimoyama M, Ota K, Kikuchi M, Yunoki K, Konda S, Takatsuki K, Ichimaru M, Tominaga S, Tsugane S, Minato K, Tobinai K, Oyama A, Hisano S, Matsumoto M, Takiguchi T, Yamaguchi K, Kinoshita K, Tajima K, Suemasu K (1988) Major prognostic factors of adult patients with advanced T-cell lymphoma/leukemia. J Clin Oncol 6:1088–1097

Tsukasaki K, Utsunomiya A, Fukuda H, Shibata T, Fukushima T, Takatsuka Y, Ikeda S, Masuda M, Nagoshi H, Ueda R, Tamura K, Sano M, Momita S, Yamaguchi K, Kawano F, Hanada S, Tobinai K, Shimoyama M, Hotta T, Tomonaga M (2007) VCAP-AMP-VECP compared with biweekly CHOP for adult T-cell leukemia-lymphoma: Japan Clinical Oncology Group Study JCOG9801. J Clin Oncol 25:5458–5464

Tsukasaki K, Hermine O, Bazarbachi A, Ratner L, Ramos JC, Harrington W, Jr, O'Mahony D, Janik JE, Bittencourt AL, Taylor GP, Yamaguchi K, Utsunomiya A, Tobinai K, Watanabe T (2009) Definition, prognostic factors, treatment, and response criteria of adult T-cell leukemia-lymphoma: a proposal from an international consensus meeting. J Clin Oncol 27:453–459

Uchiyama T, Yodoi J, Sagawa K, Takatsuki K, Uchino H (1977) Adult T-cell leukemia: clinical and hematologic features of 16 cases. Blood 50:481–492

Utsunomiya A, Miyazaki Y, Takatsuka Y, Hanada S, Uozumi K, Yashiki S, Tara M, Kawano F, Saburi Y, Kikuchi H, Hara M, Sao H, Morishima Y, Kodera Y, Sonoda S, Tomonaga M (2001) Improved outcome of adult T cell leukemia/lymphoma with allogeneic hematopoietic stem cell transplantation. Bone Marrow Transplant 27:15–20

doi:10.1186/2193-1801-3-581
Cite this article as: Kawamata *et al.*: A case of post-transplant adult T-cell leukemia/lymphoma presenting myelopathy similar to but distinct from human T-cell leukemia virus type I (HTLV- I)-associated myelopathy. *SpringerPlus* 2014 **3**:581.

Tomohiro Ishigaki*, Yuji Zaike, Masanori Nojima, Seiichiro Kobayashi, Nobuhiro Ohno, Kaoru Uchimaru, Arinobu Tojo, Hiromitsu Nakauchi and Nobukazu Watanabe

Quantification of adult T-cell leukemia/lymphoma cells using simple four-color flow cytometry

Abstract

Background: The absolute number of adult T-cell leukemia/lymphoma (ATL) cells in peripheral blood is an essential indicator to evaluate disease status. However, microscopically counting ATL cells based on morphology requires experience and tends to be inaccurate due to the rarity of ATL.

Methods: Based on our research showing that acute-type ATL cells are specifically enriched in the CD4+/CD7- (CD7N) fraction, a new analytical method to accurately quantify ATL cells was established using an internal bead standard and simple four-color flow cytometry. This method was verified by comparison with microscopic examination of 49 peripheral blood samples and used to follow up patients.

Results: A strong correlation was observed between the number of CD7N cells measured by flow cytometry and the number of abnormal lymphocytes measured microscopically by experienced technicians [Pearson's R, 0.963; Spearman's rho, 0.921; intercorrelation coefficient, 0.962]. The linear regression coefficient was close to 1 (β=1.013). Our method could detect 1 cell/μL, and the limit of quantitation was between 2.9 and 9.8 cells/μL. The frequency of CD7N cells among CD4+ cells changed during chemotherapy, which reflected differences between chemosensitive and chemoresistant cases. Kaplan-Meier analysis with a log-rank test showed that patients with decreased CD7N proportion after chemotherapy had significantly longer disease-specific survival (p=0.003).

Conclusions: Our newly established method quantified tumor cells in patients with acute-type ATL. Furthermore, this method was useful for assessing the efficacy of chemotherapy, and the change of the CD7N proportion could be more important to predict prognosis.

Keywords: adult T-cell leukemia/lymphoma (ATL); flow cytometry; HAS-Flow; human T-cell leukemia virus type 1 (HTLV-1).

DOI 10.1515/cclm-2014-0183
Received February 19, 2014; accepted June 18, 2014

***Corresponding author: Tomohiro Ishigaki,** Clinical FACS Core Laboratory, Institute of Medical Science, University of Tokyo, 4-6-1 Shirokanedai, Minato-ku, Tokyo 108-8639, Japan, Phone: +81 3 5449 5765, Fax: +81 3 5449 5750, E-mail: ishigaki@ims.u-tokyo.ac.jp; and Institute of Medical Science, Division of Stem Cell Therapy, University of Tokyo, Tokyo, Japan
Yuji Zaike: Institute of Medical Science, Department of Laboratory Medicine, Research Hospital, University of Tokyo, Tokyo, Japan
Masanori Nojima: Institute of Medical Science, Division of Advanced Medicine Promotion, University of Tokyo, Tokyo, Japan
Seiichiro Kobayashi: Institute of Medical Science, Division of Molecular Therapy, University of Tokyo, Tokyo, Japan
Nobuhiro Ohno and Kaoru Uchimaru: Institute of Medical Science, Department of Hematology and Oncology, Research Hospital, University of Tokyo, Tokyo, Japan
Arinobu Tojo: Institute of Medical Science, Division of Molecular Therapy, University of Tokyo, Tokyo, Japan; and Institute of Medical Science, Department of Hematology and Oncology, Research Hospital, University of Tokyo, Tokyo, Japan
Hiromitsu Nakauchi: Institute of Medical Science, Division of Stem Cell Therapy, University of Tokyo, Tokyo, Japan
Nobukazu Watanabe: Clinical FACS Core Laboratory, Institute of Medical Science, University of Tokyo, Tokyo, Japan

Introduction

Adult T-cell leukemia/lymphoma (ATL) is a mature T-cell neoplasm caused by human T-cell leukemia virus type 1 (HTLV-1). According to the classification of the Japanese Lymphoma Study Group (Shimoyama classification) [1], ATL is classified into four subtypes: smoldering, chronic, lymphoma, and acute-type. Chemotherapy should be offered to patients with acute, lymphoma, and chronic-type ATL with unfavorable prognostic factors.

A quantitative analysis of ATL cells is essential to evaluate the therapeutic effect. The number of ATL cells is currently estimated based on morphological abnormalities. Cells with abnormally hyperlobulated nuclei, which are termed 'flower cells', are characteristic ATL cells, but ATL cells are not always typical flower cells. ATL cells are morphologically diverse among cases, and the histological feature of ATL is diffuse proliferation of abnormal cells that vary in size and shape [2]. As discriminating ATL cells

morphologically from other lymphocytes, particularly from reactive atypical lymphocytes, is difficult, experience is required. Consequently, these difficulties cause differences between examiners and errors; therefore, morphological quantification of ATL cells tends to be inaccurate.

Many researchers have attempted to develop other counting methods or to identify markers that reflect the number of ATL cells [3–9]. The most prevalent method is HTLV-1 proviral load (PVL), measured by quantitative real-time polymerase chain reaction [5–9]. Although PVL in peripheral blood mononuclear cells (PBMCs) is a surrogate marker of the number of HTLV-1-infected cells, it has several problems. First, PVL can be affected by the total number of PBMCs, as it is only expressed as a percentage in PBMCs and not an absolute value. Second, PVL reflects only the burden of infection and is not specific for ATL cells. Third, PVL may overestimate the frequency of ATL cells when ATL cells harbor multiple copies within a single cell [5]. Furthermore, PVL measurements vary widely among laboratories, and should be standardized [10]. Finally, the method is time-consuming and is not sufficiently easy to use frequently for clinical testing. Therefore, establishing a new method to quantify ATL cells more accurately and easily is required.

We assessed a number of samples from patients with ATL using 12-color flow cytometry, and have established the flow cytometric method named 'HAS (HTLV-1 Analyzing System)-Flow,' to analyze ATL cells. Downregulation of CD3 and CD7 is observed in ATL cells, and we reported that CD4-positive cells in patients with ATL can be classified into three groups of: $CD3^{positive}/CD7^{positive}$ (CD7P), $CD3^{dimly\ positive}/CD7^{dimly\ positive}$ (CD7D), and $CD3^{dimly\ positive}/CD7^{negative}$ (CD7N) [11]. Examining the PVL showed that HTLV1-infected cells were concentrated mainly in the CD7N fraction in patients with acute-type ATL. Moreover, the Vβ repertoire revealed that tumor cells are specifically enriched in the CD7N fraction, usually to almost 100% after assessing clonality in the context of the T-cell receptor [11]. Therefore, the number of CD7N cells reflects the number of ATL cells. We applied these findings to a new clinical test, and established a new analytical method using simple four-color flow cytometry.

Materials and methods

Patient samples

Peripheral blood samples were collected from patients with acute-type ATL who were admitted to the Research Hospital at the Institute of Medical Science, University of Tokyo (IMSUT) between June 2011 and December 2012. Some of the patients were transferred to our hospital after a few courses of chemotherapy. This study was approved by the Research Ethics Committee of IMSUT, and written informed consent was obtained from all patients in accordance with the Declaration of Helsinki. All patients were diagnosed with acute-type ATL according to Shimoyama's criteria [1] and had not received hematopoietic stem cell transplantation (HSCT). In total, 49 samples from 14 patients were collected before treatment or just before a course of chemotherapy (Table 1). The effectiveness of chemotherapy was evaluated using the ATL response criteria [12].

Sample preparation and immunofluorescence staining

Peripheral blood was obtained in Vacutainer Hemogard Plus tubes (BD Biosciences, San Jose, CA, USA) by conventional venipuncture. As the volume required for our method was only 100 µL, the rest of peripheral blood samples used for routine laboratory tests were applied for measurement. A ProCOUNT method using Trucount tubes (BD Biosciences), in which a known number of fluorescent reference beads are included, was adopted to measure the absolute number of cells. First, fluorescently labeled antibodies, consisting of fluorescein isothiocyanate (FITC)-CD4 (BioLegend, San Diego, CA, USA), phycoerythrin (PE)-CD7 (BD Pharmingen, San Jose, CA, USA), allophycocyanin (APC)-CD3 (BioLegend), and PerCP-Cy5.5-CD14 (BioLegend), were mixed in a Trucount tube. Then, 100 µL of whole peripheral blood were added to the tube and mixed well. The cells were stained for 15 min at room temperature. After staining, 1 mL of Cell Lysis Buffer (BD Biosciences) was added to lyse the red blood cells. After 15 min, the sample was vortexed gently for 10 s and analyzed with a FACSCalibur flow cytometer (BD Immunocytometry Systems, San Jose, CA, USA) as soon as possible.

Sorting, cytospin, and Wright-Giemsa staining

A FACS Aria II SORP flow cytometer (BD Immunocytometry Systems) was used for cell sorting. Sorted cells were fixed on glass slides by cytospinning (20×g, 5 min) and subjected to Wright-Giemsa staining.

Flow cytometric analysis

Flow cytometry data were analyzed with FlowJo 9.6 (Treestar, San Carlos, CA, USA). We defined CD4-positive cells according to the gating procedure shown in Figure 1. The first gate on the FSC versus SSC plot was set relatively wide so as not to miss lymphocytes (Figure 1A), because adjacent monocytes and hemolytic debris could be excluded by subsequent CD14-negative selection (Figure 1B) and CD4-positive selection steps (Figure 1C). Purified CD4-positive cells were drawn in a pseudo-color plot (Figure 1E) and in a contour plot (Figure 1F). The borders among CD7P, CD7D, and CD7N in the CD7 versus CD3 plot were drawn according to contour lines (Figure 1F). Reference beads were gated in the PE versus FITC plot, according to the manufacturer's instructions (Figure 1D).

Table 1 Forty-nine samples from 14 patients with acute-type ATL were analyzed.

Patient ID	Age	Sex	Number of analysis	Average interval of analysis (range)	At the first flow cytometric evaluation					CD3 expression of ATL cells	HSCT before/during analysis
					CD7P, /μL	CD7D, /μL	CD7N, /μL	WBC, /μL	Normal lymphocytes, %	Abnormal lymphocytes, %	
1	62	M	2	14	12.9	36.4	538.0	2340	7.0	38.0	Dim	–
2	38	F	3	38.5 (14–63)	247.8	92.9	15,144.9	25,020	5.7	71.2	Dim	–
3	43	M	4	28.0 (13–43)	81.1	173.6	200.9	10,790	7.4	2.4	Dim	–
4	69	M	4	25.0 (14–40)	63.4	60.7	116.9	3450	7.5	3.0	Dim	–
5	62	M	4	17.7 (14–20)	68.0	172.7	838.5	11,310	8.5	8.5	Dim	–
6	62	M	2	27	907.7	5214.6	13,191.0	27,230	8.4	65.4	Dim	–
7	63	F	7	44.5 (30–57)	116.2	26.8	544.6	3620	12.4	21.4	Dim	–
8	67	M	6	36.2 (12–53)	189.5	266.4	290.3	10,280	15.3	3.8	Dim	–
9	50	M	6	30.0 (14–54)	86.3	112.9	6442.3	19,050	3.3	33.0	Dim	–
10	50	M	1	–	21.7	52.8	142.7	3800	10.3	3.0	Dim	–
11	44	M	1	–	683.8	184.4	6815.1	22,840	11.0	33.0	Negative	–
12	59	M	3	27.5 (27–28)	312.9	480.3	1951.4	7550	16.0	38.0	Dim	–
13	72	M	4	28.0 (25–32)	129.6	28.9	397.8	11,520	4.0	5.5	Dim	–
14	63	M	2	29	167.1	164.0	115.7	4590	23.5	1.0	Dim	–

HSCT, hematopoietic stem cell transplantation

The absolute number of cells was accurately calculated from the ratio of beads to cells in the region of the interest (Figure 1G). For example, when the total number of beads in a Trucount tube was 52187, the number of CD7N cells in the case in Figure 1 was calculated as follows: CD7N cells=(5482/100)×(52187/5201)=550.1/μL.

Validation of the flow cytometric quantification

Cryopreserved PBMCs of acute-type ATL patients were used for validation of this assay, and CD4+CD7N cells were quantified in the same way indicated above. As a blank control, phosphate buffered saline (PBS) was used. The intra-assay variation was assessed by calculating the coefficient of variation (CV) with 10 different density gradients ranging from 0 to 30000 cells/μL. Each sample was assayed six times. The limits of detection (LoD) and quantitation (LoQ) were also assessed. The LoQ was determined by the lowest concentration whose six replicates had a CV <20%. The inter-assay variation was assessed by calculating the CV of multiple determinations of a same sample measured on different days.

Conventional assessment of morphologically abnormal lymphocytes

When samples were examined by flow cytometry, total white blood cell (WBC) counts (normal range, 3500–9100/μL) were performed mechanically using an XE-2100 system (Sysmex, Kobe, Japan), and 300–400 WBCs per sample were classified by clinical technicians who were skilled in morphologically classifying ATL cells. Abnormal lymphocytes were classified according to the guideline of Japanese Association of Medical Technologists (JAMT). Briefly, lymphocytes with nuclear abnormalities, such as lobulated nuclei, multiple nuclei, evident nucleoli, or high nucleo-cytoplasmic ratio, were classified as abnormal lymphocytes. The absolute number of morphologically abnormal lymphocytes was calculated by multiplying their percentage by the total number of WBCs.

Measurement of LDH and sIL-2R

Disease status was also followed by lactate dehydrogenase (LDH) and soluble IL-2 receptor (sIL-2R). LDH activities were measured by the lactate-to-pyruvate assay according to the recommendations of the Japanese Society of Clinical Chemistry (normal range, 106–211 IU/L). Serum sIL-2R levels were measured by ELISA (normal range, 145–519 U/mL).

Statistical analysis

The correlation between the number of CD7N cells measured by flow cytometry and the number of abnormal lymphocytes measured by microscopic counting was assessed by Pearson's correlation coefficients (R), Spearman's correlation coefficients (rho), intra-class correlation coefficients (ICC), and linear regression coefficients.

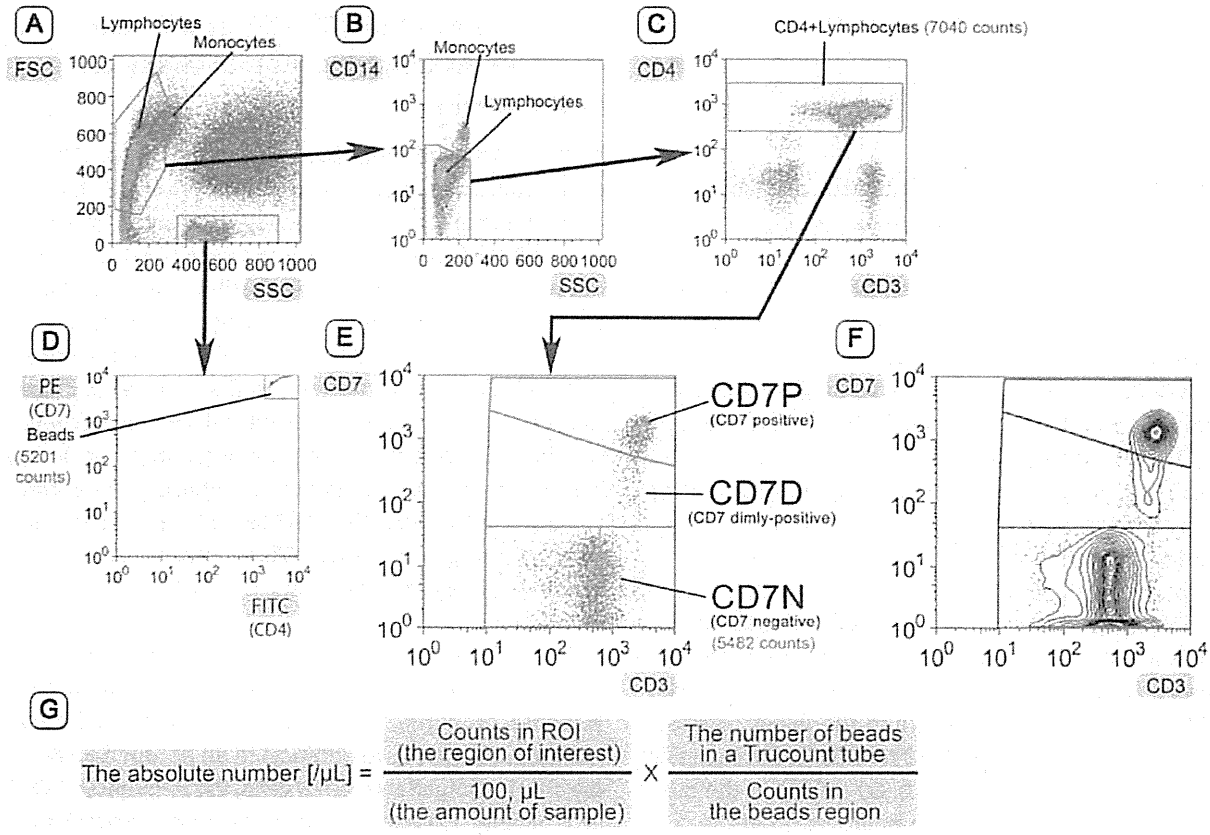

Figure 1 Flow cytometric gating procedure.
CD4-positive cells were properly defined according to the procedure shown here (A–C). CD4-positive cells were classified into CD7P, CD7D, and CD7N cells according to the contour lines of a CD7 versus CD3 plot (E, F). Reference beads were gated in the PE versus FITC plot (D). The absolute number of CD7N cells was calculated using this formula (G).

As data from both measurements followed a log-normal distribution, these analyses were performed after log-transformation. Bland-Altman analysis was used to calculate the agreement between flow cytometric and microscopic counting. In addition, the inverse probability weighting (IPW) method and mixed model (varying intercepts and slopes) were used due to the imbalance in sample number and individual differences between the patients. Kaplan-Meier analysis with a post hoc log-rank test was performed for disease-specific survival stratified by whether relative decrease of the CD7N proportion after the chemotherapy was over 5% or not. Statistical analyses were performed using the GraphPad Prism software, ver. 6.0c (GraphPad Software Inc., San Diego, CA, USA) and SPSS software ver. 20 (IBM Corp., Armonk, NY, USA).

Results

Abnormal lymphocytes are enriched in the CD7N fraction

Along with our previous research using 12-color flow cytometry, simple four-color flow cytometry could classify CD4-positive lymphocytes into three groups of: CD7P, CD7D, and CD7N (Figure 1). Almost all of CD7-negative cells were dimly-positive for CD3, except for a case in which CD7-negative cells were all negative for CD3. In the representative case of acute-type ATL where the proportions of CD7P, CD7D, and CD7N in CD4+ cells were 2.7%, 1.7%, and 95.6%, the proportions of abnormal lymphocytes in these three fractions were 0.0%, 6.0%, and 99.0%, respectively. Morphological evaluation showed that almost all CD7N cells were morphological abnormal, whereas none of the CD7P cells were abnormal.

Intra- and inter-assay variation of this flow cytometric quantification was low

To evaluate the precision of our assay, we assessed the intra-assay CVs of 10 different density gradients. The intra-assay CVs of samples with the average of 1.2, 2.9, 9.8, 20.5, 42.7, 442.7, 1073.7, 8081.2, and 30,729.8 cells/μL were 30.69, 31.17, 5.94, 4.89, 3.64, 4.02, 4.61, 2.45, and 4.98%, respectively. Six determinations of a blank control were all measured to be

0 cells/μL. The limit of detection was about 1 cell/μL, and the limit of quantitation was estimated to be between 2.9 and 9.8 cells/μL. The inter-assay CV was 5.81%.

Correlation between CD7N cells and morphologically abnormal lymphocytes

We found a significant correlation between the number of CD7N cells and the number of morphologically abnormal lymphocytes (Pearson's R=0.963, Spearman's ρ=0.921, and ICC=0.962; Figure 2A). Moreover, the linear regression coefficient was close to 1 [β=1.013, 95% confidence interval (CI), 0.991–1.034]. The calculated number of CD7N cells was often similar to the number of morphologically abnormal lymphocytes. In two cases, flow cytometric analysis detected ATL cells but microscopic counting did not.

In addition, we reassessed the correlation using the IPW method and the mixed model considering the imbalance in sample number and individual differences between patients. Using the IPW method, Pearson's R=0.973, Spearman's ρ=0.942, and the linear regression coefficient was 1.010 (95% CI 0.990–1.030). The regression coefficient was 0.979 (95% CI 0.893–1.064) in the mixed model. Almost all results were improved from the crude analysis, and the influences of sampling imbalance and individual differences were limited.

The Bland-Altman plot showed good agreement between both measurements (Figure 2B). There seemed to be little additive or proportional bias.

The change in the CD7-CD3 profile was useful to evaluate the effectiveness of chemotherapy

We then compared the change in a CD7 versus CD3 plot of CD4-positive cells during chemotherapy between chemoresistant and chemosensitive cases. The proportion of CD7N cells in chemoresistant cases increased or did not change, although the absolute number of CD7N cells decreased slightly. In the case of Figure 3A, i.e., both the number of ATL cells and lactate dehydrogenase (LDH) decreased after the first course of chemotherapy, and the response seemed good. Nevertheless, the CD7-CD3 profile was almost unchanged. After the second course, all parameters, including the number of ATL cells and the LDH and soluble interleukin (IL)-2 receptor levels, increased. The disease was not controlled by chemotherapy, and the patient died after 1 month.

In contrast, the CD7-CD3 profile changed dramatically in clinically good responders who achieved a complete response or partial response. Representative data are shown in Figure 3B. In addition to an abrupt decrease in the absolute number of CD7N cells, the frequency of CD7N cells among CD4-positive cells decreased significantly, whereas the frequency of CD7P cells increased. While a significant proportion of patients with acute-type ATL cannot undergo HSCT because of uncontrollable disease, the patient in Figure 3B received allogeneic HSCT after several courses of chemotherapy.

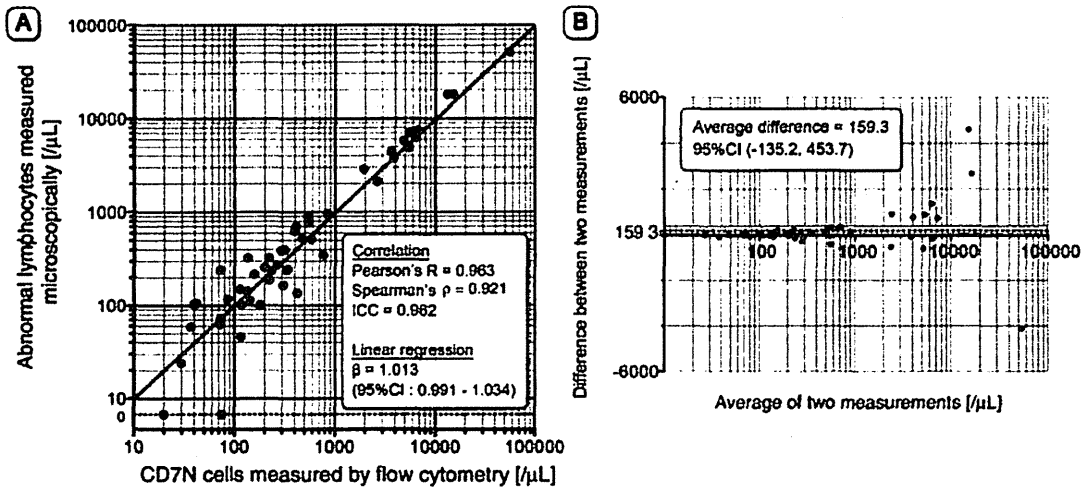

Figure 2 The correlation between CD7N cells and abnormal lymphocytes.
The correlation between CD7N cells measured by flow cytometry and abnormal lymphocytes measured microscopically was evaluated using three correlation tests and a linear regression analysis (A). The agreement between the two measurements was analyzed with a Bland-Altman plot (B).

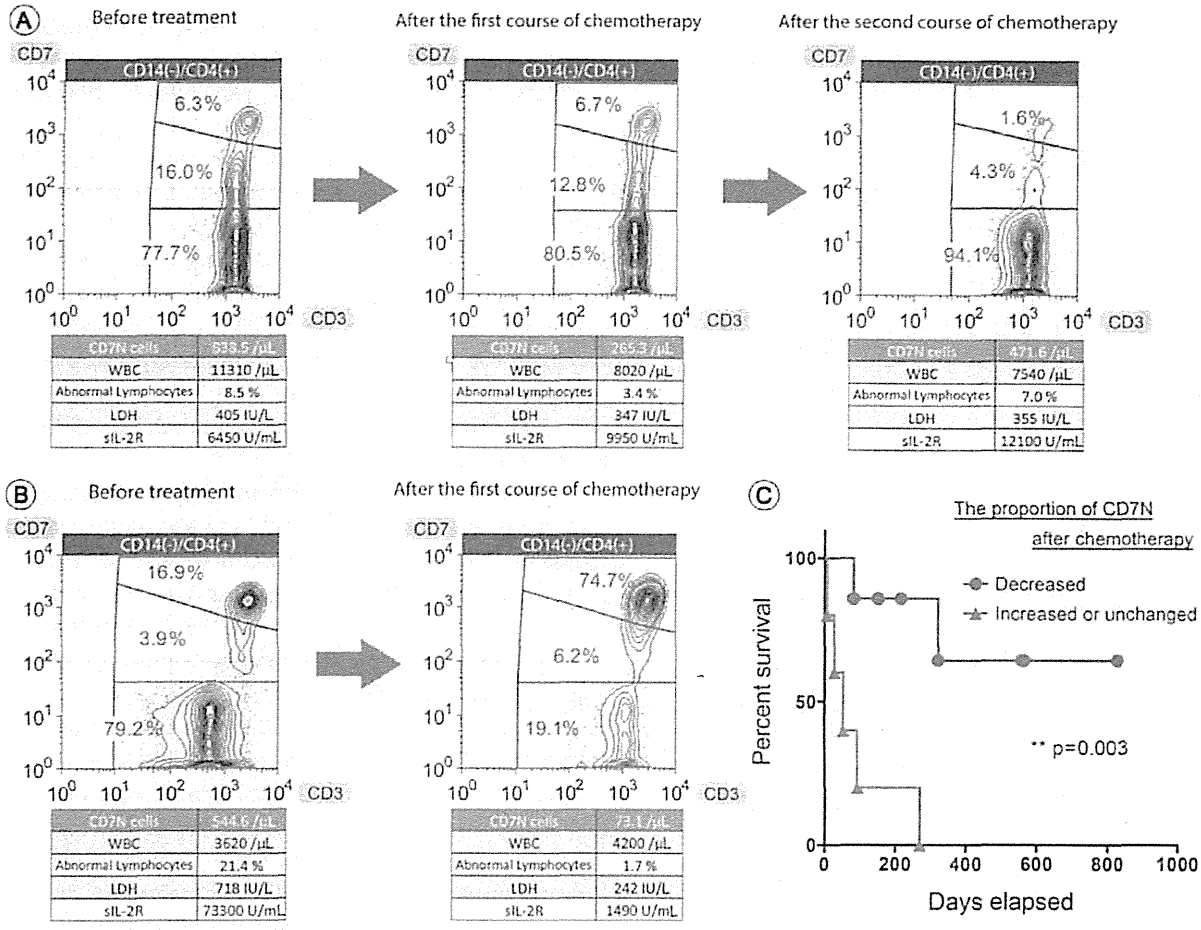

Figure 3 The CD7-CD3 profile allowed for an assessment of chemotherapy efficacy and could predict prognosis.
A patient with an almost unchanged CD7-CD3 profile after the first course of chemotherapy had an unfavorable prognosis after the second course (A). In contrast, a patient that showed a good clinical response to chemotherapy exhibited marked changes in the CD7-CD3 profile after only one course of chemotherapy (B). Kaplan-Meier suvival curves showed ATL patients with decreased CD7N proportion after chemotherapy showed significantly longer disease-specific survival (p=0.003) (C).

The pattern of change in the CD7-CD3 profile was observed repeatedly in many patients to reflect the effectiveness of chemotherapy, and these results suggested that the change in the CD7-CD3 profile is useful to assess the effect of chemotherapy.

ATL patients with decreased CD7N proportion after chemotherapy showed longer disease-specific survival

Next, we focused on the first chemotherapy during flow cytometric analyses periods, and examined the relation between the prognosis and the change of clinical parameters (Table 2). Consequently, the CD7N proportion was picked up, and acute-type ATL patients were classified into two groups by the relative change of the CD7N proportion after the chemotherapy. The CD7N proportion was considered decreased when a relative decrease of more than 5% was achieved after chemotherapy compared with the one before the chemotherapy. ATL patients with decreased CD7N proportion after chemotherapy showed longer survival than ones with unchanged or increased (Figure 3C). A log-rank test showed that there was a significant difference between the two groups (p=0.003). The difference suggested that the change in the CD7N proportion could be more important to predict the prognosis.

Discussion

Based on our previous studies [11, 13], we applied research findings to a clinical test. We made the procedure as simple as possible to maximize practicality after several

Table 2 The change of clinical parameters after the first chemotherapy.

Patient ID	Before chemotherapy				After chemotherapy				Change of CD7N proportion after chemotherapy	HSCT after flow cytometric analysis	Outcome (days after post-chemotherapy evaluation)
	Proportion of CD7N, %	Absolute number of CD7N, /μL	LDH, IU/L	sIL-2R, U/mL	Proportion of CD7N,%	Absolute number of CD7N, /μL	LDH, IU/L	sIL-2R, U/mL			
1	91.6	538.0	774	22,600	96.1	115.2	651	-	Increased	-	Died of ATL (7)
2	97.8	15,144.9	272	24,100	97.4	5479.9	108	27,700	Unchanged	-	Died of ATL (93)
3	44.1	200.9	376	4200	37.6	72.8	273	7420	Decreased	+	Died of ATL (322)
4	48.5	116.9	446	4040	60.7	181.2	717	22,200	Increased	-	Died of ATL (28)
5	77.7	838.5	405	6450	80.5	265.3	347	9950	Increased	-	Died of ATL (54)
6	68.3	13,191.0	633	11,700	57.9	2640.0	283	3500	Decreased	+	Died of ATL (83)
7	79.2	544.6	718	73,300	19.1	73.1	242	1490	Decreased	+	Alive in CR (828)
8	38.9	290.3	259	3500	30.9	796.5	200	2300	Decreased	-	Died of infection (152)[a]
9	97.0	6442.3	655	17,200	96.2	3859.2	392	21,400	Unchanged	+	Died of ATL (270)
12	71.1	1951.4	582	15,500	65.2	577.1	238	2840	Decreased	+	Alive in CR (565)
13	71.5	397.8	251	6340	59.6	335.6	169	1420	Decreased	-	Alive in CR (559)
14	25.9	115.7	293	5230	14.3	29.7	452	7820	Decreased	-	Transferred to another hospital (217)[a]

[a]ATL was under control when patients were censored.

trials, and finally established a practical flow cytometry method to quantify acute-type ATL cells.

Flow cytometry is highly sensitive in detecting minimal residual disease (MRD) of hematological malignancies. Similar flow cytometric approach for detection of MRD in ATL was reported previously, and a multi-parametric approach using CD2, CD3, CD4, CD5, CD7, CD25, CD26, and CD27 was useful for detection of ATL cells [14]. We established here a more practical and easier flow cytometric method using only CD3, CD4, CD7, and CD14. Moreover we limited the use to acute-type ATL cases because our previous studies showed the expression of cell surface antigens on ATL cells was slightly different among subtypes.

Combination of gates is also important and characteristic of our method. We showed here all the procedures including gating and quantification so that the method could be easily applied in other hospitals. This test provides accurate quantification of CD7N lymphocytes achieved by establishing an appropriate gating procedure (Figure 1). As a first gate, two methods are generally used to gate lymphocytes. One is FSC versus SSC gating, and the other is CD45 versus SSC gating [15]. The latter method is often used to analyze malignant hematologic diseases and eliminate red blood cell debris but is not convenient to analyze ATL cells because these occasionally lose [16] or express a high level of CD45. Therefore, we applied FSC versus SSC gating for lymphocyte gating. Moreover, eliminating monocytes is necessary to precisely enumerate CD7N lymphocytes because monocytes are weakly positive for CD4 and negative for CD7. Hence, we gated out monocytes carefully by CD14 staining before CD4-positive selection. Combination of the first wide lymphocyte gate and the following two strict gates enabled purification of CD4-positive lymphocytes without excess or deficiency. Then, CD7N cells were defined according to the contour lines in a plot of CD4-positive lymphocytes. Drawing the border between CD7D and CD7N cells was easy because contour lines clearly and horizontally separated these two populations. In contrast, the border between CD7P and CD7D cells was sometimes difficult to determine; thus, further improvement may be needed. However, the latter border is not necessary to estimate the number of ATL cells using this method.

Although the number of ATL cells is currently estimated based on morphologically abnormal cells, morphological evaluation of ATL cells often differs between examiners. Particularly, morphological enumeration by inexperienced examiners tends to be inaccurate. We therefore assessed here the correlation between the number of CD7N cells and the number of morphologically

abnormal lymphocytes evaluated only by experienced technicians (Figure 2A). As expected, a strong correlation was identified. It is noteworthy that the regression coefficient was very close to 1.0. This new flow cytometric method is useful for accurate evaluation of ATL cells. Furthermore, only flow cytometry detected ATL cells in two cases. As the validation study of the assay showed very low limits of detection and quantitation, flow cytometry could detect ATL cells more sensitively than microscopic counting.

The Bland-Altman plot also showed good agreement and the relatively small average difference between the two measurements (Figure 2B). However, the three samples with the highest WBCs had high differences between the two methods. While flow cytometry allows rapid and accurate analysis of a much larger number of cells, manual counting has limitations in accuracy and the number of counts. Since the absolute number of morphologically abnormal lymphocytes was calculated by multiplying their percentage by the total number of WBCs, the margin of error in microscopic counting tended to get larger as the number of WBCs got higher. Although the relative differences between the two methods were generally not so high, these findings suggested the number of abnormal lymphocytes in samples with high WBC counts should be carefully examined.

This flow cytometry-based method has many advantages compared to PVL. First, flow cytometry allows for calculation of the absolute number of ATL cells, which is not affected by the number of other cells. Second, intra- and inter-assay variations of our method were confirmed to be low. The inter- and intra-laboratory variabilities of the ProCOUNT method are also known to be low [17]. Therefore, this flow cytometric method is precise and can be easily standardized. Third, it is practical and takes no more than 1 h.

In addition to its usefulness for quantitation, we also found that the change in the CD7-CD3 profile discriminated cases sensitive to chemotherapy and may predict prognosis (Figure 3A and B). Serum sIL-2R and LDH levels are also clinically important [18, 19], but they are not as specific for disease status because they are influenced by other factors, such as infection, inflammation, and hemolysis. Patients with a better prognosis tended to have a markedly better change in the CD7-CD3 profile after only one course of chemotherapy. In contrast, cases with unchanged or worse CD7-CD3 profiles after one course of chemotherapy tended to have an unfavorable prognosis after the second course, even if the number of ATL cells decreased, or the levels of sIL-2R and LDH improved initially.

From various parameters of the CD7-CD3 profile, we had tried picking up prognostic indicators. We focused on the first chemotherapy, and examined the change of various clinical parameters (Table 2) and their relation with survival. Needless to say, the number of CD7N cells, as the number of ATL cells, was important to evaluate the disease status through the follow-up, and robust reduction of the number of CD7N cells was necessary for a better prognosis. However, the change of the CD7N proportion seemed more sensitive. We examined the relationship between the disease-specific survival and the relative change of the CD7N proportion after chemotherapy. Although the number of patients was limited, it is noteworthy that patients with decreased CD7N proportion had significantly longer survival (Figure 3C). Further accumulation of cases and longer follow-up are warranted to elucidate the ability of this method to predict prognosis.

Our experience suggests that this method can be applied to almost all patients with acute-type ATL. However, some limitations should be noted. First, this method did not accurately detect ATL cells in patients who had undergone HSCT, as downregulation of CD7 in CD4-positive non-ATL lymphocytes was observed in most cases [20]. Second, this method cannot identify ATL cells in rare cases in which ATL tumor cells lack CD4 expression or express CD7. Therefore, a brief confirmation of the ATL phenotype using other surface markers is recommended before flow cytometric quantification.

In summary, we established a clinical test to accurately quantify ATL cells in patients with acute-type ATL using simple four-color flow cytometry. This newly established clinical application of 'HAS-Flow' will provide more accurate enumeration of ATL cells and assessment of chemosensitivity.

Acknowledgments: We would like to thank Dr. Naoki Oyaizu and Dr. Naoyuki Isoo (Laboratory Medicine, Research Hospital, Institute of Medical science) for their kind permission to introduce this clinical test, as well as Mr. Yukihisa Tanaka, Ms. Etsuko Nagai, and Ms. Motoko Mizukami for their excellent morphological classification.
Author contributions: All the authors have accepted responsibility for the entire content of this submitted manuscript and approved submission.
Research funding: None declared.
Employment or leadership: None declared.
Honorarium: None declared.
Competing interests: The funding organization(s) played no role in the study design; in the collection, analysis, and interpretation of data; in the writing of the report; or in the decision to submit the report for publication.

References

1. Shimoyama M. Diagnostic criteria and classification of clinical subtypes of adult T-cell leukaemia-lymphoma. A report from the Lymphoma Study Group (1984–87). Br J Haematol 1991;79:428–37.
2. Ohshima K. Pathological features of diseases associated with human T-cell leukemia virus type I. Cancer Sci 2007;98:772–8.
3. de Souza JG, Fonseca FG, Martins-Filho OA, Teixeira-Carvalho A, Martins CP, Carvalho LD, et al. Diagnostic tool based on an HTLV-1-Tax expression system in eukaryotic cells using a poxvirus vector. J Virol Methods 2010;166:65–71.
4. Sadamori N. Clinical and biological significance of serum tumor markers in adult T-cell leukemia. Leuk Lymphoma 1996;22:415–9.
5. Kamihira S, Dateki N, Sugahara K, Hayashi T, Harasawa H, Minami S, et al. Significance of HTLV-1 proviral load quantification by real-time PCR as a surrogate marker for HTLV-1-infected cell count. Clin Lab Haematol 2003;25:111–7.
6. Waters A, Oliveira AL, Coughlan S, de Venecia C, Schor D, Leite AC, et al. Multiplex real-time PCR for the detection and quantitation of HTLV-1 and HTLV-2 proviral load: addressing the issue of indeterminate HTLV results. J Clin Virol 2011;52:38–44.
7. Moens B, Lopez G, Adaui V, Gonzalez E, Kerremans L, Clark D, et al. Development and validation of a multiplex real-time PCR assay for simultaneous genotyping and human T-lymphotropic virus type 1, 2, and 3 proviral load determination. J Clin Microbiol 2009;47:3682–91.
8. Takenouchi H, Umeki K, Sasaki D, Yamamoto I, Nomura H, Takajo I, et al. Defective human T-lymphotropic virus type 1 provirus in asymptomatic carriers. Int J Cancer 2011;128:1335–43.
9. Altamirano NA, Rocco C, Aulicino P, Sen L, Mangano A. Quantitation of HTLV-I proviral load by a real-time PCR assay using SYBR Green: comparison of two methods for DNA isolation. J Virol Methods 2010;170:160–4.
10. Kamihira S, Yamano Y, Iwanaga M, Sasaki D, Satake M, Okayama A, et al. Intra- and inter-laboratory variability in human T-cell leukemia virus type-1 proviral load quantification using real-time polymerase chain reaction assays: a multi-center study. Cancer Sci 2010;101:2361–7.
11. Tian Y, Kobayashi S, Ohno N, Isobe M, Tsuda M, Zaike Y, et al. Leukemic T cells are specifically enriched in a unique CD3(dim) CD7(low) subpopulation of CD4(+) T cells in acute-type adult T-cell leukemia. Cancer Sci 2011;102:569–77.
12. Tsukasaki K, Hermine O, Bazarbachi A, Ratner L, Ramos JC, Harrington W Jr., et al. Definition, prognostic factors, treatment, and response criteria of adult T-cell leukemia-lymphoma: a proposal from an international consensus meeting. J Clin Oncol 2009;27:453–9.
13. Kobayashi S, Tian Y, Ohno N, Yuji K, Ishigaki T, Isobe M, et al. The CD3 versus CD7 plot in multicolor flow cytometry reflects progression of disease stage in patients infected with HTLV-I. PLoS One 2013;8:e53728.
14. Shao H, Yuan CM, Xi L, Raffeld M, Morris JC, Janik JE, et al. Minimal residual disease detection by flow cytometry in adult T-cell leukemia/lymphoma. Am J Clin Pathol 2010;133:592–601.
15. Borowitz MJ, Guenther KL, Shults KE, Stelzer GT. Immunophenotyping of acute leukemia by flow cytometric analysis. Use of CD45 and right-angle light scatter to gate on leukemic blasts in three-color analysis. Am J Clin Pathol 1993;100:534–40.
16. Weil R, Levraud JP, Dodon MD, Bessia C, Hazan U, Kourilsky P, et al. Altered expression of tyrosine kinases of the Src and Syk families in human T-cell leukemia virus type 1-infected T-cell lines. J Virol 1999;73:3709–17.
17. Schnizlein-Bick CT, Spritzler J, Wilkening CL, Nicholson JK, O'Gorman MR. Evaluation of TruCount absolute-count tubes for determining CD4 and CD8 cell numbers in human immunodeficiency virus-positive adults. Site Investigators and The NIAID DAIDS New Technologies Evaluation Group. Clin Diagn Lab Immunol 2000;7:336–43.
18. Motoi T, Uchiyama T, Uchino H, Ueda R, Araki K. Serum soluble interleukin-2 receptor levels in patients with adult T-cell leukemia and human T-cell leukemia/lymphoma virus type-I seropositive healthy carriers. Jpn J Cancer Res 1988;79:593–9.
19. Araki K, Harada K, Nakamoto K, Shiroma M, Miyakuni T. Clinical significance of serum soluble IL-2R levels in patients with adult T cell leukaemia (ATL) and HTLV-1 carriers. Clin Exp Immunol 2000;119:259–63.
20. Leblond V, Othman TB, Blanc C, Theodorou I, Choquet S, Sutton L, et al. Expansion of CD4+CD7- T cells, a memory subset with preferential interleukin-4 production, after bone marrow transplantation. Transplantation 1997;64:1453–9.

Supplemental Material: The online version of this article (DOI: 10.1515/cclm-2014-0183) offers supplementary material, available to authorized users.

Cancer Science
Japanese Cancer Association JCA
Open Access

Epigenetic deregulation of *Ellis Van Creveld* confers robust Hedgehog signaling in adult T-cell leukemia

Ryutaro Takahashi,[1,6] Makoto Yamagishi,[1,6] Kazumi Nakano,[1] Toshiko Yamochi,[2] Tadanori Yamochi,[1] Dai Fujikawa,[1] Makoto Nakashima,[1] Yuetsu Tanaka,[3] Kaoru Uchimaru,[4] Atae Utsunomiya[5] and Toshiki Watanabe[1]

[1]Graduate School of Frontier Sciences, The University of Tokyo, Tokyo; [2]Department of Pathology, Showa University School of Medicine, Tokyo; [3]Department of Immunology, Graduate School of Medicine, University of the Ryukyus, Okinawa; [4]Institute of Medical Science, The University of Tokyo, Tokyo; [5]Department of Hematology, Imamura Bun-in Hospital, Kagoshima, Japan

Key words

ATL, epigenetics, EVC, Hedgehog, HTLV-1

Correspondence

Toshiki Watanabe, Laboratory of Tumor Cell Biology, Department of Medical Genome Sciences, Graduate School of Frontier Sciences, The University of Tokyo, 4-6-1 Shirokanedai, Minato-ku, Tokyo 108-8639, Japan.
Tel: +81-3-5449-5298; Fax: +81-3-5449-5418;
E-mail: tnabe@ims.u-tokyo.ac.jp

[6]These authors contributed equally to this study.

Funding information

JSPS KAKENHI (24790436). (23390250). MEXT KAKENHI (221S0001). Ministry of Health, Labour and Welfare H24-Third Term Cancer-004 Uehara Memorial Foundation.

Received April 14, 2014; Revised June 20, 2014; Accepted July 1, 2014

Cancer Sci **105** (2014) 1160–1169

doi: 10.1111/cas.12480

One of the hallmarks of cancer, global gene expression alteration, is closely associated with the development and malignant characteristics associated with adult T-cell leukemia (ATL) as well as other cancers. Here, we show that aberrant overexpression of the *Ellis Van Creveld* (EVC) family is responsible for cellular Hedgehog (HH) activation, which provides the pro-survival ability of ATL cells. Using microarray, quantitative RT-PCR and immunohistochemistry we have demonstrated that EVC is significantly upregulated in ATL and human T-cell leukemia virus type I (HTLV-1)-infected cells. Epigenetic marks, including histone H3 acetylation and Lys4 trimethylation, are specifically accumulated at the *EVC* locus in ATL samples. The HTLV-1 Tax participates in the coordination of EVC expression in an epigenetic fashion. The treatment of shRNA targeting EVC, as well as the transcription factors for HH signaling, diminishes the HH activation and leads to apoptotic death in ATL cell lines. We also showed that a HH signaling inhibitor, GANT61, induces strong apoptosis in the established ATL cell lines and patient-derived primary ATL cells. Therefore, our data indicate that HH activation is involved in the regulation of leukemic cell survival. The epigenetically deregulated EVC appears to play an important role for HH activation. The possible use of EVC as a specific cell marker and a novel drug target for HTLV-1-infected T-cells is implicated by these findings. The HH inhibitors are suggested as drug candidates for ATL therapy. Our findings also suggest chromatin rearrangement associated with active histone markers in ATL.

Adult T-cell leukemia (ATL) is a malignant T-cell disorder caused by infection with a human retrovirus, human T-cell leukemia virus type I (HTLV-1).[1–3] The prognosis of aggressive types of ATL is poor.[4] At present, ATL is an intractable disease in human beings. To prevent the development of ATL and the poor prognosis that is associated with it, the development of effective therapies based on the molecular characteristics is needed.

To explore effective drugs, precise understanding of the molecular mechanism of ATL pathogenesis is essential. We have previously reported that genetic and epigenetic imbalances and following aberrant gene expressions are the main framework for ATL tumor cells.[5,6] In addition, the involvement of systemic downregulation of cellular microRNA has been implicated in the leukemogenesis of ATL. So far, several host cellular signaling abnormalities induced by HTLV-1 Tax in the early phase of infection[6–8] and the aberrant activation of nuclear factor-kappa B (NF-κB) contribute to ATL leukemogenesis.[9,10] Although other several molecular deregulations have been suggested in ATL, we have not completely covered the landscape of signaling networks in ATL.

Recently, Hedgehog (HH) signaling has been reported as an oncogenic pathway in many types of cancers.[11,12] Constitutive HH activation leads to the overproliferation or survival of several cancer cells, such as basal cell carcinoma or B-cell lymphomas.[13–15] There are some HH inhibitors under clinical trial as drug candidates against those cancers.[16]

In the present study, using ATL patient samples and some ATL models, we found two specific gene overproductions in ATL, *Ellis Van Creveld syndrome 1* (*EVC1*) and *EVC2*, which belong to the EVC family of genes that are implicated in HH regulation.[17–19] We demonstrated that epigenetically upregulated EVC was associated with cellular HH activity. *EVC* and other regulatory factors for HH signaling were responsible for the survival of ATL cell lines and also primary ATL samples. Direct evidence from the ATL samples revealed that universal epigenetic marks associated with actively transcribed genes were rearranged in the leukemic cells. These findings may shed light on the abnormal gene expression signature and leukemic cell traits observed in ATL.

Materials and Methods

Patient samples. The primary peripheral blood mononuclear cells (PBMC) from ATL patients and healthy volunteers were a part of those collected with informed consent as a collaborative project of the Joint Study on Prognostic Factors of ATL Development (JSPFAD). The project was approved by the University

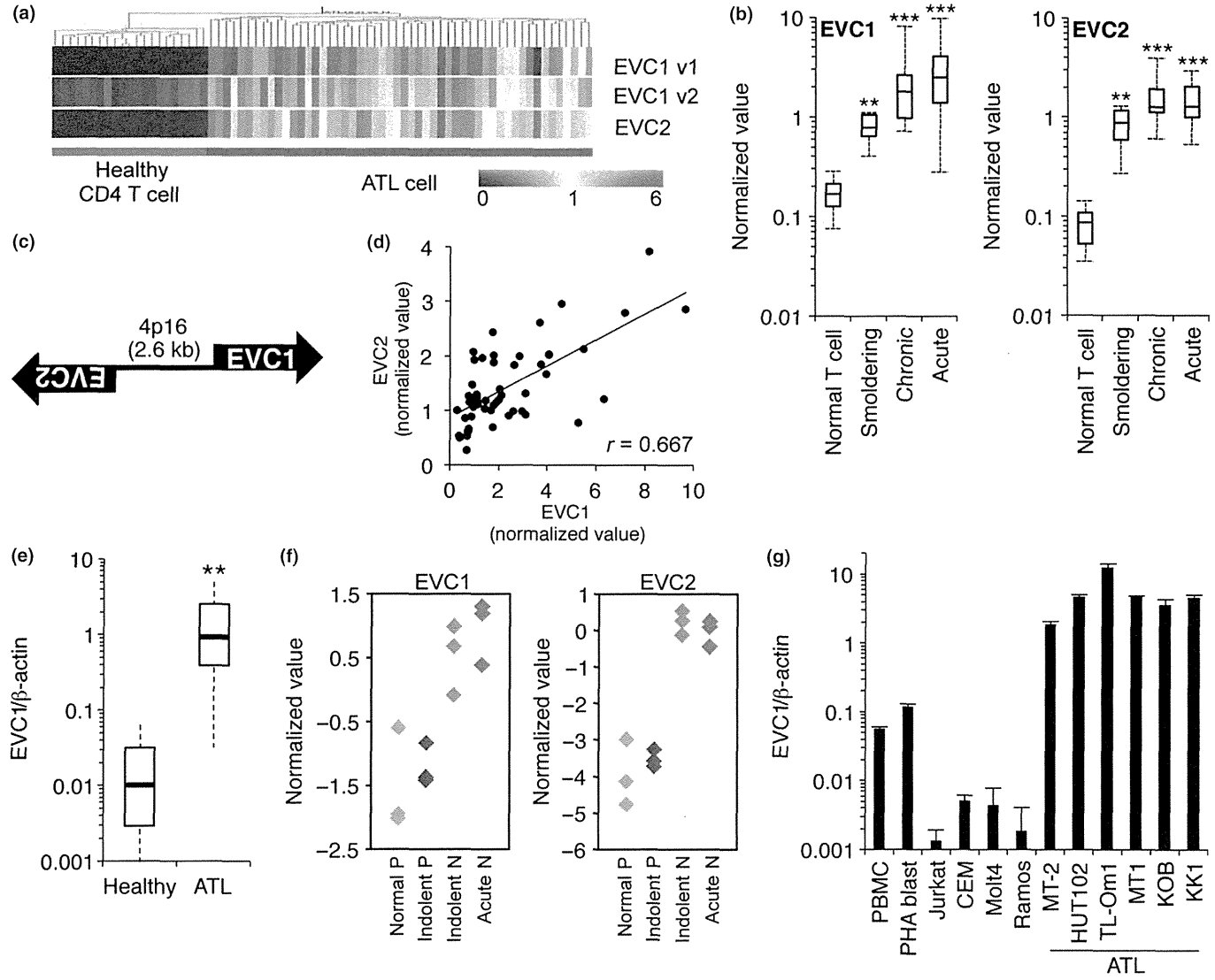

Fig. 1. *EVC* overexpression in ATL. (a, b) Microarray heatmap (a) and box plot (b) of *EVC*. $^{**}P < 0.01$. $^{***}P < 0.001$. (c) Schematic illustration of locus encoding *EVC1/2*. (d) Individual expression values ($n = 52$) between *EVC1* and *EVC2*. (e) *EVC1* mRNA level in ATL patient PBMC (total, $n = 11$; acute, $n = 7$; chronic, $n = 4$) and in CD4+ T cells from healthy donors ($n = 6$) evaluated using quantitative RT-PCR (qRT-PCR). $^{**}P < 0.01$. (f) *EVC1* and *EVC2* levels in CADM1 versus CD7 plot subpopulations. Normal P, CD4+/CADM1−/CD7+ T cells from healthy donors; Indolent P, CD4+/CADM1−/CD7+ from indolent ATL patients; Indolent N, CD4+/CADM1+/CD7− from indolent ATL patients; Acute N, CD4+/CADM1+/CD7− from acute ATL patients. The gene expression microarray dataset is available in Kobayashi *et al.*[25] (g) *EVC1* levels in various cell lines examined using qRT-PCR ($n = 3$, mean ± SD).

of Tokyo and Showa University research ethics committees. The PBMC were isolated using Ficoll separation and maintained in RPMI1640 (Invitrogen, Carlsbad, CA, USA) supplemented with 1% of self-serum and antibiotics (Invitrogen). Clinical information is shown in the Supporting Information Methods.

Microarray analysis. Gene expression profiling of ATL patient samples and normal CD4+ T cells has been performed previously.[5] The coordinate has been deposited in the Gene Expression Omnibus database (GSE33615).

Cell culture. The HTLV-1-infected cell lines MT-2 and HUT102, ATL-derived cells MT-1 and TL-Om1, and other leukemic cell lines were cultured in RPMI1640 with 10% FCS. ATL-derived KOB and KK1 were cultured in RPMI1640 with 10% FCS and 10 ng/mL recombinant human IL-2 (R&D Systems, Minneapolis, MN, USA). The 293T cell was cultured in DMEM with 10% FCS. All cell lines were cultured at 37°C, with 5% CO_2.

Plasmids and HH activity analysis. Tax-encoding plasmids have been described previously.[20] *EVC1* cDNA was amplified as two fragments from the human cDNA library. Cellular HH activity was evaluated using a dual-luciferase assay (Promega, Madison, WI, USA).[21] Briefly, 7 × GLI binding site (GACACCCA)-luciferase plasmid and control RSV-Renilla plasmid were co-transfected into target cells using Lipofectamine2000 (Invitrogen). At 24 h post-transfection, the cells were collected and analyzed using a dual-luciferase assay.

Quantitative RT-PCR. Procedures for RNA isolation and RT-PCR have been described previously.[5] Primer sets for quantitative RT-PCR (qRT-PCR) are provided in the Supporting Information Methods.

Epigenetic analyses. Bisulfite treatment was conducted using a MethylEasy Xceed Rapid DNA Bisulphite Modification kit (Human Genetic Signatures, NSW, Australia). For evaluating histone covalent modifications, a chromatin immunoprecipita-

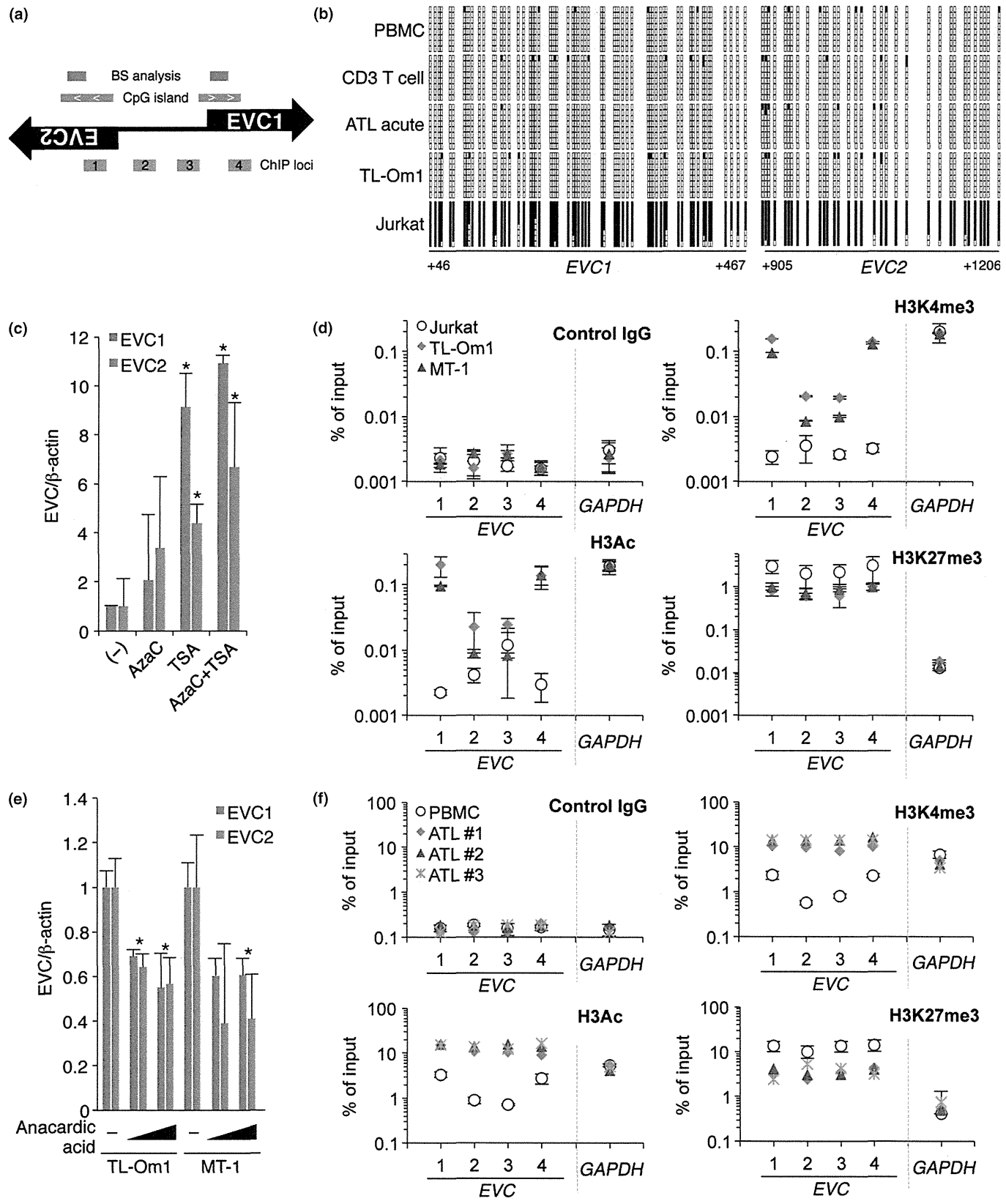

Fig. 2. Epigenetic reprogramming in the *EVC* locus. (a) Schematic of CpG islands and chromatin immunoprecipitation (ChIP) loci. (b) Results of bisulfite sequencing (+46 to +466 from *EVC1* transcription start site [TSS]; +905 to +1206 from *EVC2* TSS). The black and empty boxes represent methylated and unmethylated CpG, respectively. (c) *EVC* RNA levels in Jurkat cells in the presence or absence of epigenetic drugs ($n = 3$, mean ± SD). $^*P < 0.05$. (d) Histone covalent modifications at *EVC* and *GAPDH* loci in three cell lines were analyzed using PCR-based ChIP assay with specific antibodies. Positions of primer sets for the real-time PCR are indicated in (a). Enrichment values relative to input samples are plotted. (e) TL-Om1 and MT-1 cells were treated with 1 or 5 μM of anacardic acid for 48 h and the *EVC* mRNA level was then analyzed ($n = 3$, mean ± SD). $^*P < 0.05$. (f) Epigenetic changes in primary ATL samples. Three independent clinical samples were compared with normal PBMC ($n = 3$, mean ± SD).

tion (ChIP) assay was conducted as described previously.[5,22] Anti-H3K4me3 (#9751S; Cell Signaling, Danvers, MA, USA), anti-AcH3 (#06-599; Millipore, Billerica, MA, USA), anti-H3K27me3 (#39155; Active Motif, Carlsbad, CA, USA) and control IgG (I5381; SIGMA, St. Louis, MO, USA) were used for ChIP. Primers for the qPCR are provided in the Supporting Information Methods.

Immunohistochemistry. For preparation of the paraffin block of 293T cells, the cells were fixed in 20% of formalin/PBS for 24 h. After removing the formalin, alcohol dehydration and paraffin permeation were done using Tissue-Tek VIP5Jr (Sakura, Alphen aan den Rijn, The Netherlands). Paraffin blocks were sectioned at 3-μm thickness. The sections were then transferred to coating slide glasses (Muto pure chemicals, Bunkyo-ku, Tokyo, Japan). After paraffin removal, the paraffin sections of the 293T and ATL cells were treated with 3% H_2O_2. Antigen-retrieval treatment was done using Histofine antigen retrieval solution pH9 (Nichirei, Chuo-Ku, Tokyo, Japan) for 20 min under microwave radiation. After reaction with the first antibody, anti-EVC antibody (HPA008703, 1:400; SIGMA), and the second antibody (K5027, ENVISION Kit/HRP [DAB]; Dako, Bunkyo-ku, Tokyo, Japan), the sections were colored using ENVISION Kit/HRP [DAB] DAB+ (K3468; DAKO). Finally, the sections were stained with hematoxylin.

Lentivirus construction and production. Detailed procedures for lentivirus production have been described previously.[5] Briefly, replication-defective, self-inactivating lentivirus vectors were used.[23,24] shRNA were cloned into a CS-H1-EVBsd. High-titer viral solutions prepared using a centrifugation-based concentration were transduced into ATL cell lines using the spinoculation method. The transduced cells were

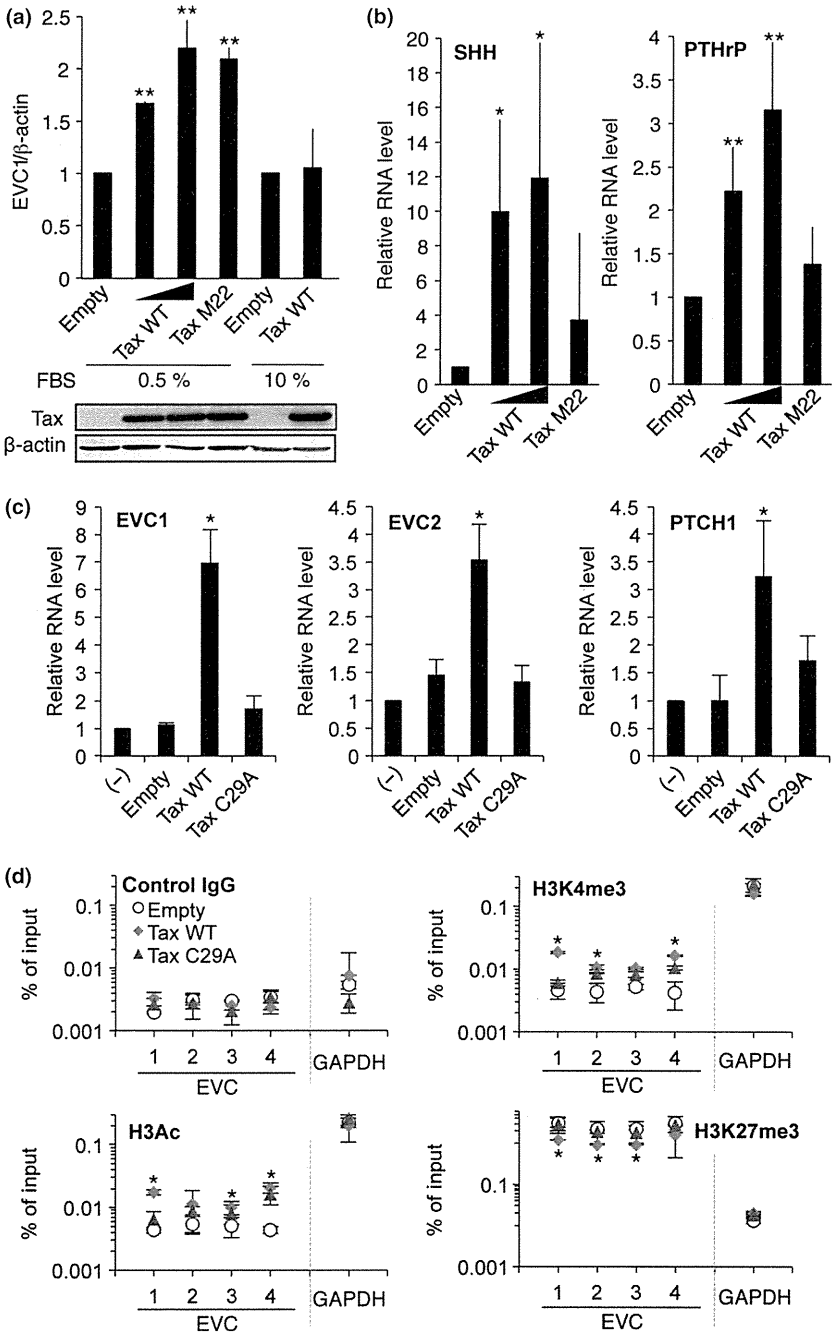

Fig. 3. Role of Tax in *EVC* regulation. (a) *EVC1* RNA levels are affected by Tax. The 293T cells in different FBS condition were transfected with the indicated plasmids. Relative *EVC1* levels were evaluated using quantitative RT-PCR (qRT-PCR) (top panel, $n = 3$, mean ± SD). $^{**}P < 0.01$. Tax expression was confir-med using western blotting with an anti-Tax antibody (Lt-4) (bottom panel). (b) Levels of *SHH* and *PTHrP* in the presence or absence of Tax ($n = 3$, mean ± SD). $^{*}P < 0.05$. $^{**}P < 0.01$. (c) *EVC* and *PTCH1* levels in Jurkat cells expressing Tax ($n = 3$, mean ± SD). $^{*}P < 0.05$. (d) Tax-mediated epigenetic changes. Histone modifications at *EVC* and *GAPDH* loci in Tax-expressing Jurkat cells were analyzed using a ChIP assay. $^{*}P < 0.05$ (Tax WT *vs* Empty). Primer positions are shown in Figure 2(a).

further selected by blastcidin and used within 14 days. shRNA sequences are described in the Supporting Information Methods.

Cell viability and apoptosis analyses. For the cell proliferation assay, 5000 cells were plated in a 96-well flat bottom plate with RPMI1640 medium supplemented with 1% FCS. After 1–3 days culture, cell numbers were evaluated using Cell Counting kit-8 (Dojindo, Kumamoto, Japan). The apoptosis cell was determined using PE Annexin V/7-AAD stainings (BD Pharmingen, San Jose, CA, USA). Detection of apoptotic cells was performed using FACSCalibur (Becton, Dickinson, Franklin Lakes, NJ, USA). Primary ATL cells were defined using sequential gating based on a Forward scatter/Side Scatter (FSC/SSC) pattern and a CD4-positive population (anti-CD4-FITC; BD Pharmingen). Collected data were analyzed using FlowJo software (Tree Star, Ashland, OR, USA).

Results

Epigenetic abnormalities in *EVC* regulation in ATL. We have determined the gene expression signature of ATL tumor cells by conducting massive microarrays.[5] The gene expression profiles from 52 ATL patients and 21 healthy donors identified a large number of specific gene upregulations in ATL cells. Among these, the genes encoding EVC1 and EVC2 were strikingly overexpressed in ATL patient samples, which had a relationship to disease progression (Fig. 1a,b). These genes are located in an identical chromosome *4p16*, under a bi-directional promoter (Fig. 1c), and their expressions have shown a strong positive correlation (Fig. 1d). The qRT-PCR revealed that the median of the *EVC1* mRNA level in ATL was 90.9-fold higher than that of normal CD4+ T-cells (Fig. 1e). Specificity of tumor-associated EVC expression was confirmed using the dataset from CADM1 versus CD7 plot subpopulation samples.[25] CADM1 expression and CD7 loss have recently been identified as highly sensitive molecular markers of HTLV-1-infected cells. *EVC1* and *EVC2* were significantly expressed in the CADM1+/CD7− tumorous population (Fig. 1f). The HTLV-1-infected and ATL-derived cells showed higher levels of *EVC1* mRNA compared with those in other leukemia and lymphoma cell lines and those of healthy PBMC (Fig. 1g). The MT-2 and HUT102 cells, which highly express HTLV-1 genes, showed high *EVC1* mRNA levels similar to those in ATL-derived cells.

Looking at the tumor-associated epigenetic reprogramming that was frequently observed in ATL,[5,6] we analyzed the epigenetic status of the *EVC* locus to clarify the possible

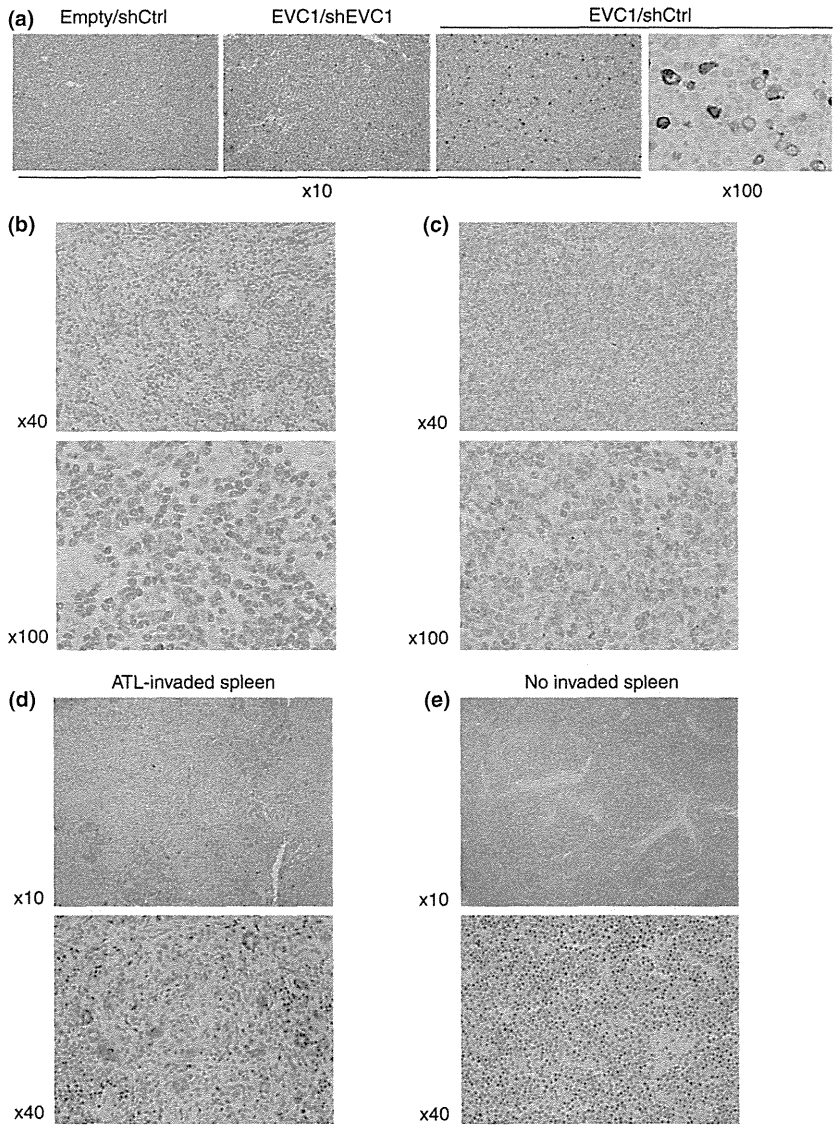

Fig. 4. EVC1 expression in ATL cells. (a–e) Immunohistochemistry-based EVC1 protein detection in paraffin-embedded samples: 293T transfected with the indicated plasmids (a), primary ATL lymph node (b, c, representative data are shown) and spleen from mice engrafted with primary ATL cells (d, tumor invasive, $n = 3$; e, non-invasive). These samples were stained with anti-EVC1 antibody and hematoxylin.

involvement of epigenetic variation in *EVC* deregulation. There were two typical CpG islands in the *EVC* locus whose transcription may be tightly regulated by the gain of CpG methylation (Fig. 2a). However, bisulfite sequencing revealed that DNA methylation was not acquired in normal lymphocytes, as well as in the primary ATL sample (Fig. 2b). CpG hypermethylation within the *EVC* locus was found only in Jurkat cells where the *EVC* expression was nearly undetectable (Fig. 1g). Instead, treatment with epigenetic drugs, particularly a histone deacetylase (HDAC) inhibitor tricostatin A (TSA), reactivated the *EVC* transcription in Jurkat cells, suggesting that histone modifications such as acetylation were involved in *EVC* regulation (Fig. 2c). To further address the epigenetic implication, we performed ChIP assays to assess the possible contribution of histone modification in *EVC* upregulation. The ATL cell lines showed significant accumulation (log-scale) of histone H3 acetylation (H3Ac) and H3K4 trimethylation (H3K4me3), which have been recognized generally as positive transcription marks around the transcription start site region of both *EVC1* and *EVC2* (Fig. 2d). Treatment with a pan-histone acetylase inhibitor, anacardic acid, reduced *EVC* transcription in ATL cell lines (Fig. 2e). Interestingly, H3K27me3, which has been implicated as a poor prognostic marker in ATL,[5,26] was decreased at the *EVC* locus in ATL cells. We confirmed directly the epigenetic reprogramming at the *EVC* locus in primary ATL samples (Fig. 2f). In summary, it appeared that the acquisition of active histone modifications and the reciprocal disappearance of H3K27me3 contributed to aberrant EVC transcription.

Role of HTLV-1 Tax in *EVC* transcription. Next we addressed whether Tax could participate in the deregulated *EVC1* transcription. Although Tax expression did not influence the *EVC1* mRNA levels in 293T cells at complete growth conditions, Tax activated *EVC1* transcription in a dose-dependent manner in serum-starved conditions (Fig. 3a). A NF-κB activation-defected Tax mutant, M22,[27] showed similar *EVC1* induction, suggesting that *EVC1* transcriptional activation was independent from NF-κB activation. Indeed, the pharmacological inhibition of NF-κB activity failed to prevent *EVC* transcription in ATL cell lines (data not shown). Meanwhile, Tax induced transcription of *Sonic hedgehog* (*Shh*), which encodes the HH activation ligand, in a NF-κB-dependent manner (Fig. 3b). The experimental condition was validated by the evaluation of *PTHrP*, which has been known to be a Tax and NF-κB-targeted gene. HTLV-1 *HBZ* did not affect *EVC* transcription (Supporting Information Fig. S1).

We examined the possible relationship between Tax and histone modifications. For this purpose, we established lentiviral vectors inducing stable Tax expression in Jurkat cells. More than 80% of transduction efficiencies were achieved in all tested cells. Tax induced transcription of *EVC1* and *EVC2*, as well as the HH target gene *PTCH1* (Fig. 3c). Interestingly, the Tax C29A mutant, which was unable to localize in the nucleus,[28] failed to induce *EVC*, suggesting that *EVC* induction was directly caused by the nuclear-localized Tax. A ChIP assay revealed that the Tax wild type, but not the C29A mutant, directly accumulated H3K4me3 and H3Ac in the *EVC* locus (Fig. 3d). Thus, Tax appeared to, at least partially, induce *EVC* expression through epigenetic reprogramming.

EVC1 expression in primary ATL cell. We performed immunohistochemistry (IHC) with a commercially available antibody that recognized EVC1. First, we stained paraffin-embedded 293T cells transduced with the EVC1-expressing plasmid to test the antibody specificity. Strong positivity was detected in the plasmid-transduced sample but not in samples with untreated or concomitantly treated with shRNA targeting *EVC1* (Fig. 4a). Using this antibody we investigated EVC1 expression in several aggressive ATL cases. Most ATL cases showed stable EVC1 positivity (7/8, 87.5%; two representatives in Fig. 4b,c). We noted that all EVC1-positive cells were dysplastic. Furthermore, EVC1 expression was clearly detected in a mouse ATL model that was established using xenotrans-

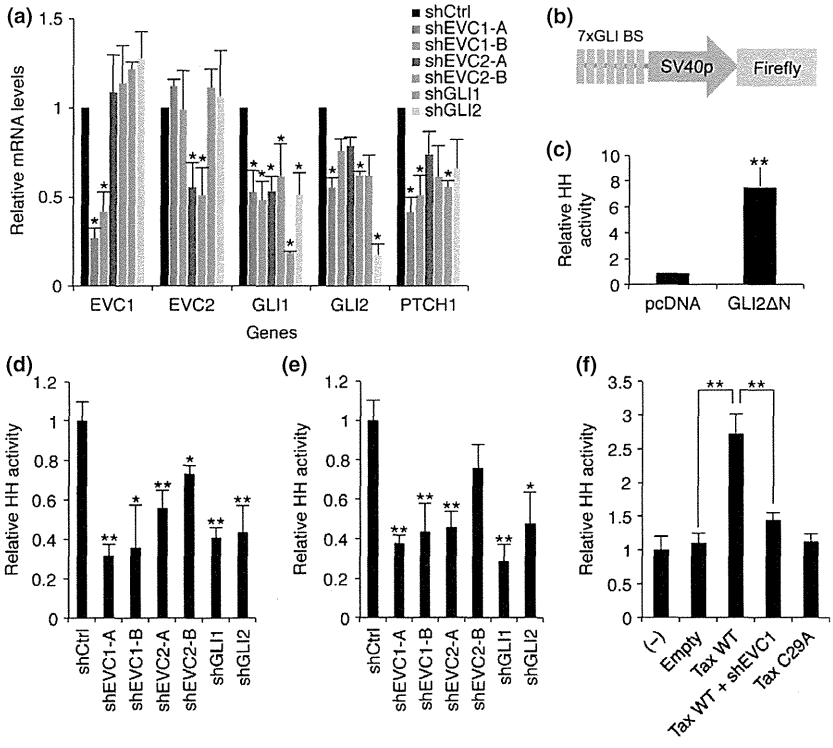

Fig. 5. EVC supports Hedgehog (HH) activity. (a) Relative RNA levels in shRNA-expressing TL-Om1 cells ($n = 3$, mean ± SD). $^*P < 0.05$. (b) Luciferase reporter plasmid containing 7 × sequential GLI-binding sites. (c) GLI2ΔN activa-ted HH activity ($n = 3$, mean ± SD). $^{**}P < 0.01$. (d–f) Hedgehog activity in various shRNA-expressing TL-Om1 (d), MT-2 (e) and Tax and shEVC1-expressing Jurkat (f) ($n = 3$–4, mean ± SD). $^*P < 0.05$. $^{**}P < 0.01$.

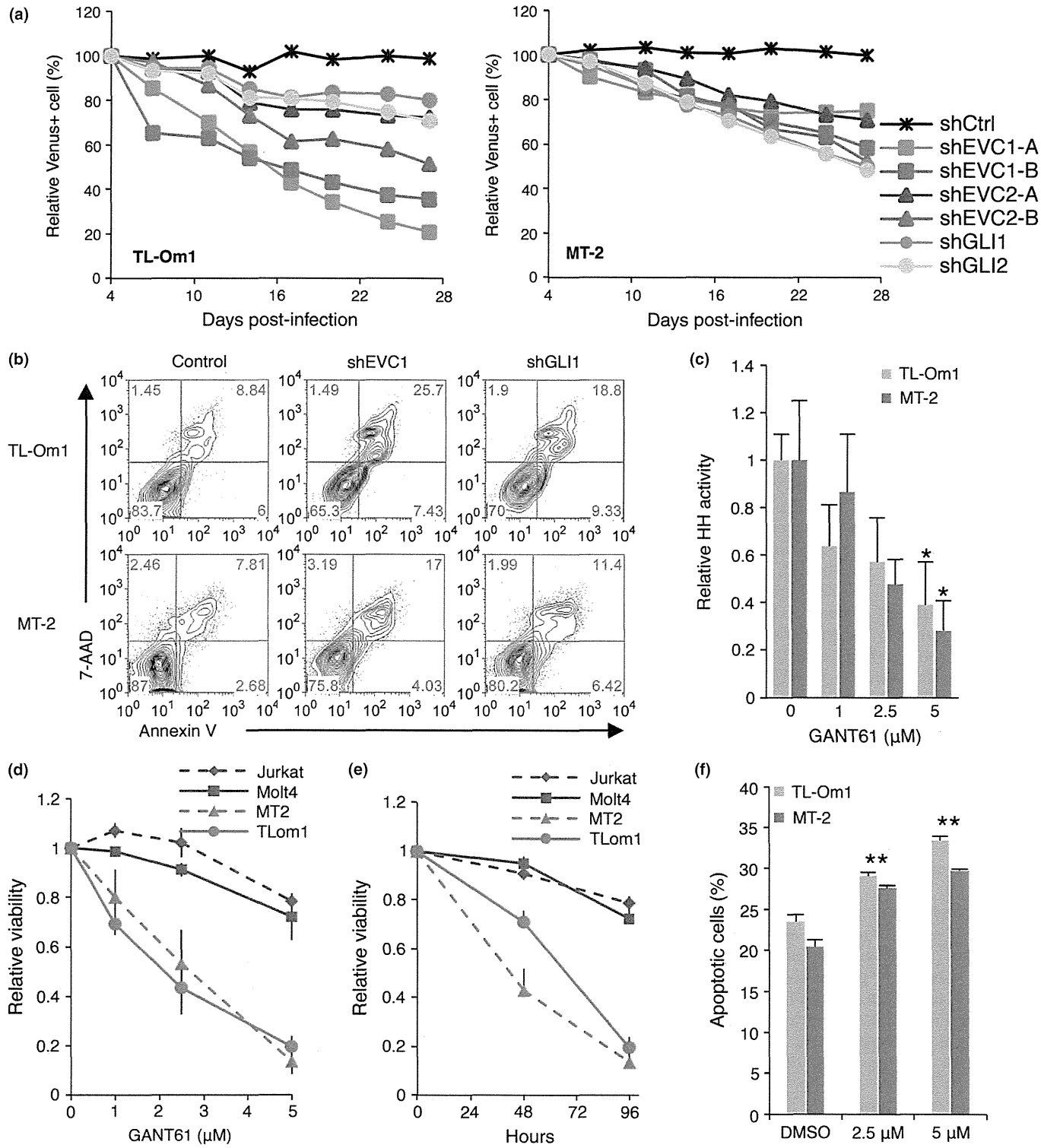

Fig. 6. Hedgehog (HH)-dependent ATL cell survival. (a) Time course of the abundance of Venus+ TL-Om1 (left) and MT-2 (right) infected with lentiviral vector expressing control shRNA (shCtrl), either of two shRNA targeting EVC1 and EVC2, or shRNA targeting GLI1 and GLI2, then cultured for 27 days together with uninfected cells. Data are representative of three independent experiments. Results are presented relative to those of cells at 4 days post-infection. (b) shRNA-mediated apoptosis induction. shRNA-expressing cells were cultured in 1% FBS for 72 h. The apoptotic pattern was defined by gating with Venus+ and Annexin V/7-AAD ($n = 3$, representative data). (c) GANT61 inhibited HH activity in ATL cells ($n = 3$, mean ± SD). $^*P < 0.05$. (d–e) GANT61 reduced ATL cell viability ($n = 3$, mean ± SD). The cells were treated with the indicated concentrations of GANT61 for 96 h (d) or with 5 μM of GANT61 for the indicated time periods (e). Cells were maintained in 1% FCS. (f) GANT61-dependent apoptosis analyzed using Annexin V/7-AAD staining ($n = 3$, mean ± SD). $^{**}P < 0.01$.

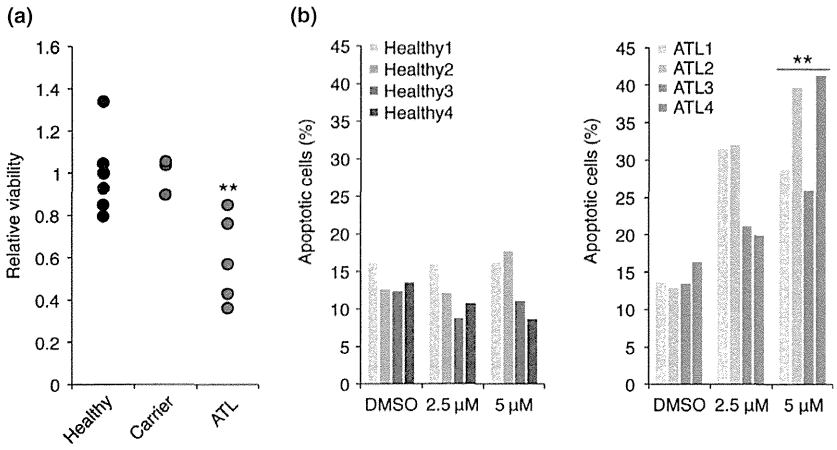

Fig. 7. GANT61 treatment reduced cell viabilities of primary ATL samples. (a) Effect of GANT61 in primary PBMC samples. The PBMC from healthy donors ($n = 7$), asymptomatic carriers ($n = 3$) and ATL patients ($n = 5$) were exposed in 5 μM of GANT61 for 72 h. Cells were maintained in media with 1% self-serum. $^{**}P < 0.01$. (b) GANT61-dependent apoptosis in ATL samples. The PBMC from healthy donors ($n = 4$) and ATL patients ($n = 4$) were treated with 5 μM of GANT61 for 72 h. Graphs show percentiles of apoptotic population in CD4+ cells $^{**}P < 0.01$.

plantation of primary tumor cells derived from an ATL patient. The lymphoma cells specifically expressed EVC1 (Fig. 4d,e). Taken together, EVC1 protein was definitely expressed in ATL cells.

EVC in HH activation. The EVC family has been implicated in HH signaling.[18,19] We performed the knockdown of EVC in TL-Om1 and MT-2 cells, which all highly expressed EVC (Fig. 1g). Specific knockdown was accomplished using lentivirus harboring specific and previously validated shRNA against EVC1, EVC2 or GLI transcription factors in the HH cascade. The qRT-PCR revealed the knockdown efficiency and also the HH activity as the RNA levels of *PTCH1* and *GLI1* were well-established HH activity markers.[29] The EVC depletion resulted in reduction of *PTCH1* and *GLI1* mRNA levels (Fig. 5a). Next we established a luciferase reporter containing 7 × sequential GLI-binding sites (Fig. 5b), which strongly responded against GLI2ΔN, a constitutive active form of GLI2[12] (Fig. 5c). As expected, the knockdown of EVC1 and EVC2 represented diminished HH activity in TL-Om1 and MT-2 cells (Fig. 5d,e). In addition, Tax activated the HH signal in Jurkat cells (Fig. 5f). Knockdown of EVC1 cancelled Tax-directed HH activation, suggesting that Tax affects HH signaling through, at least partially, EVC induction epigenetically.

EVC-dependent cell survival in ATL. Aberrant activation of HH provides cell survival ability in myeloma and lymphoma.[14,15] We found that different shRNA targeting EVC and GLI caused a progressive depletion of Venus+ cells (Fig. 6a). Knockdown of EVC1 or EVC2 attenuated ATL cell proliferation (Fig. S2). The growth defect was associated with a substantial decrease in the expression of targeted genes (Fig. 5). We then measured the apoptotic status by staining Annexin V/7-AAD. Specific analyses within the knocked down cells were achieved by gating with Venus fluorescence. At complete growth condition, slight but steady apoptosis was induced by EVC1 knockdown in MT-2 and TL-Om1 cells (data not shown). Furthermore, strong apoptosis was observed in EVC1-depleted cells at low FCS condition (Fig. 6b). This cell death appeared to be due to HH inactivation because GLI1-knocked down cells showed similar results.

Specific killing of ATL cell by GANT61. GANT61 is a cell-permeable hexahydropyrimidine compound, which has been shown to be a well-established inhibitor of GLI-mediated gene transactivation.[29] GANT61 treatment successfully reduced GLI binding to the target sequence (Fig. 6c). In that condition, MT-2 and TL-Om1 cells showed remarkable reduction of cell viability by GANT61 treatment in dose- and time-dependent manners (Fig. 6d,e), which may be caused by apoptosis (Fig. 6f).

Finally, we evaluated the pharmacological activity of GANT61 on primary ATL samples. Although GANT61 did not show a clear effect on PBMC derived from healthy donors and HTLV-1 carriers, its treatment specifically reduced the viability of ATL samples significantly (Fig. 7a). Flow cytometry demonstrated that GANT61 specifically killed CD4+ leukemic cells from ATL patients via apoptosis induction (Fig. 7b).

Discussion

A large number of efforts have collectively concluded that aberrant gene expression patterns contribute to the malignant characteristics in ATL and other neoplastic cells. In the present study, based on the careful analyses of patient samples, we have demonstrated that *EVC* is drastically overexpressed in mRNA and its protein can be specifically detected in ATL cells in contrast to normal CD4+ T-cells. To the best of our knowledge, this is the first report regarding EVC expression and function in lymphocytes. The results of the microarray indicate that *EVC* expression appears to be induced in accordance with disease progression. EVC1 protein expression is observed in dysplastic ATL cells derived from patients and a xenotransplantation model. Because the EVC family may be membrane-associated proteins (Fig. 4),[30] the present study provides us with the possibility that EVC expressions might be useful cell markers of HTLV-1-infected T-cells for future clinical purposes.

The EVC family has been identified initially as the responsible genes for one morphogenic disorder, Ellis van Creveld syndrome; it is also believed to play a role in the determination of body-axis or morphogenesis by usually bearing one step of the HH signaling pathway.[12,17–19] Knockout studies have demonstrated that EVC1 and EVC2 cooperatively act as positive modulators of the HH pathway in mouse fibroblasts and chondrocytes. However, abnormal EVC upregulation has not been reported in any cancers; whether the HH pathway is sensitive to cellular dynamism of EVC has not been elucidated as yet. Herein, we demonstrated that overexpression of EVC can be linked to HH activity in T cells for the first time. In addition, several experimental results, including the knockdown assay and GANT61 treatment, suggest totally that the HH pathway was activated in ATL, which in turn contributed to ATL cell survival. Further study will be required for mechanistic insights on how EVC activates HH in T cells.

Further investigation uncovered that transcription from the *EVC* locus was coordinated by epigenetic alteration. In particular, the lymphoma-associated H3Ac and H3K4me3 accumulations appeared to dominate EVC upregulation. Direct evidence from patient samples supported the epigenetic reprogramming, including previously unappreciated H3K4me3 rearrangements, conferring robust EVC expression. Interestingly, repressive histone mark H3K27me3 was mutually reduced at the *EVC* locus in the ATL samples, suggesting that cooperative regulation in this bivalent domain may define the EVC expression and possibly HH activity.

HTLV-1 Tax was involved in the regulation of EVC via epigenetic regulation. Nuclear localization-deficient Tax mutant was unable to induce EVC expression, implying that Tax may participate directly in determination of chromatin architecture. Indeed, lentiviral expression of Tax partially increased active histone modifications, which in turn activated HH signaling. Previously, we and others have reported that Tax physically binds with histone modifying factors, including HDAC,[31] SUV39H1[32] and SMYD3.[20] Interplay between Tax and epigenetic rearrangement may be closely involved in the progression of HTLV-1-infected cells to leukemic cells. Meanwhile, other ATL-specific epigenetic events including significant modifications on histone acetylation, H3K4me3 and H3K27me3 clearly dominate stable EVC expression. The alteration of the epigenetic landscape by Tax and other molecular mechanisms such as expression changes of epigenetic modifiers will be elucidated by comprehensive analysis such as a genome-wide ChIP analysis.

In the context of molecular targeting, a new possibility for the HH inhibitor was suggested. Recently, aberrant HH activation and its contribution to cell survival and the cell cycle have been reported in various cancer cells.[11,12] In agreement with other tumors where HH is active, we found that ATL was sensitive against GANT61. This compound can inhibit HH signaling by preventing DNA binding of the GLI family and has few impacts on the viability of healthy CD4+ T cells. We note that we could not confirm the EVC-directed upregulation of common HH target genes such as *Cyclin D1* and *Bcl-2* in ATL models (data not shown). Given that the HH pathway regulates transcription of many genes important for cell fate and many inhibitors against HH cascade have been developed,[16] our findings suggest that pharmacological drugs that can inhibit the HH pathway may be feasible for ATL treatment. Identification of ATL-specific HH target genes will help understanding of the HH roles in survival capability.

In summary, we have identified EVC overexpression as a specific character of ATL and HTLV-1-infected T cells. We have demonstrated the molecular mechanism that overexpressed EVC1 contributes to ATL cell survival. Considering aberrant gene expression associated with cancers, the emerging relationship between epigenetic regulation and the HH pathway provides us with conceptual advance in understanding the broad-acting oncogenic signaling.

Acknowledgments

The authors thank Dr M. Iwanaga and Ms T. Akashi for support and maintenance of JSPFAD and Mr Y. Sasaki for experimental support of the IHC study. The authors also thank Drs H. Miyoshi and A. Miyawaki for providing the Venus-encoding lentivirus vectors and Dr S. Okada for providing the NOJ mice. This work is supported by JSPS KAKENHI Grant Numbers 24790436 (M.Y.) and 23390250 (T.W.), MEXT KAKENHI Grant Number 221S0001 (T.W.), Grant-in-Aid from the Ministry of Health, Labour and Welfare H24-Third Term Cancer-004 (T.W.), and a grant from the Uehara Memorial Foundation (M.Y.).

Disclosure Statement

The authors have no conflict of interest.

References

1 Uchiyama T, Yodoi J, Sagawa K, Takatsuki K, Uchino H. Adult T-cell leukemia: clinical and hematologic features of 16 cases. *Blood* 1977; **50**: 481–92.
2 Poiesz BJ, Ruscetti FW, Gazdar AF, Bunn PA, Minna JD, Gallo RC. Detection and isolation of type C retrovirus particles from fresh and cultured lymphocytes of a patient with cutaneous T-cell lymphoma. *Proc Natl Acad Sci USA* 1980; **77**: 7415–9.
3 Yoshida M, Miyoshi I, Hinuma Y. Isolation and characterization of retrovirus from cell lines of human adult T cell leukemia and its implication in the disease. *Proc Natl Acad Sci USA* 1982; **79**: 2031–5.
4 Tsukasaki K, Utsunomiya A, Fukuda H *et al.* VCAP-AMP-VECP compared with biweekly CHOP for adult T-cell leukemia–lymphoma: Japan Clinical Oncology Group Study JCOG9801. *J Clin Oncol* 2007; **25**: 5458–64.
5 Yamagishi M, Nakano K, Miyake A *et al.* Polycomb-mediated loss of miR-31 activates NIK-dependent NF-κB pathway in adult T cell leukemia and other cancers. *Cancer Cell* 2012; **21**: 121–35.
6 Yamagishi M, Watanabe T. Molecular hallmarks of adult T cell leukemia. *Front Microbiol* 2012; **3**: 334.
7 Grassmann R, Aboud M, Jeang KT. Molecular mechanisms of cellular transformation by HTLV-1 Tax. *Oncogene* 2005; **24**: 5976–85.
8 Hall WW, Fujii M. Deregulation of cell-signaling pathways in HTLV-1 infection. *Oncogene* 2005; **24**: 5965–75.
9 Mori N, Fujii M, Ikeda S *et al.* Constitutive activation of NF-kappaB in primary adult T-cell leukemia cells. *Blood* 1999; **93**: 2360–8.
10 Watanabe M, Ohsugi T, Shoda M *et al.* Dual targeting of transformed and untransformed HTLV-1-infected T cells by DHMEQ, a potent and selective inhibitor of NF-kappaB, as a strategy for chemoprevention and therapy of adult T-cell leukemia. *Blood* 2005; **106**: 2462–71.
11 Low JA, de Sauvage FJ. Clinical experience with Hedgehog pathway inhibitors. *J Clin Oncol* 2010; **28**: 5321–6.
12 Briscoe J, Thérond PP. The mechanisms of Hedgehog signalling and its roles in development and disease. *Nat Rev Mol Cell Biol* 2013; **14**: 416–29.
13 Johnson RL, Rothman AL, Xie J *et al.* Human homolog of patched, a candidate gene for the basal cell nevus syndrome. *Science* 1996; **272**: 1668–71.
14 Dierks C, Grbic J, Zirlik K *et al.* Essential role of stromally induced hedgehog signaling in B-cell malignancies. *Nat Med* 2007; **13**: 944–51.
15 Singh RR, Kim JE, Davuluri Y *et al.* Hedgehog signaling pathway is activated in diffuse large B-cell lymphoma and contributes to tumor cell survival and proliferation. *Leukemia* 2010; **24**: 1025–36.
16 McMillan R, Matsui W. Molecular pathways: the hedgehog signaling pathway in cancer. *Clin Cancer Res* 2012; **18**: 4883–8.
17 Tompson SWJ, Ruiz-Perez VL, Blair HJ *et al.* Sequencing EVC and EVC2 identifies mutations in two-thirds of Ellis-van Creveld syndrome patients. *Hum Genet* 2007; **120**: 663–70.
18 Ruiz-Perez VL, Blair HJ, Rodriguez-Andres ME *et al.* Evc is a positive mediator of Ihh-regulated bone growth that localises at the base of chondrocyte cilia. *Development* 2007; **134**: 2903–12.
19 Dorn KV, Hughes CE, Rohatgi R. A Smoothened-Evc2 complex transduces the Hedgehog signal at primary cilia. *Dev Cell* 2012; **23**: 823–35.
20 Yamamoto K, Ishida T, Nakano K *et al.* SMYD3 interacts with HTLV-1 Tax and regulates subcellular localization of Tax. *Cancer Sci* 2011; **102**: 260–6.
21 Sasaki H, Hui C, Nakafuku M, Kondoh H. A binding site for Gli proteins is essential for HNF-3beta floor plate enhancer activity in transgenics and can respond to Shh *in vitro*. *Development* 1997; **124**: 1313–22.
22 Yamagishi M, Ishida T, Miyake A *et al.* Retroviral delivery of promoter-targeted shRNA induces long-term silencing of HIV-1 transcription. *Microbes Infect* 2009; **11**: 500–8.
23 Miyoshi H, Takahashi M, Gage FH, Verma IM. Stable and efficient gene transfer into the retina using an HIV-based lentiviral vector. *Proc Natl Acad Sci USA* 1997; **94**: 10319–23.

24 Miyoshi H, Blömer U, Takahashi M, Gage FH, Verma IM. Development of a self-inactivating lentivirus vector. *J Virol* 1998; **72**: 8150–7.
25 Kobayashi S, Nakano K, Watanabe E *et al.* CADM1 expression and stepwise downregulation of CD7 are closely associated with clonal expansion of HTLV-I-infected cells in adult T-cell leukemia/lymphoma. *Clin Cancer Res* 2014; **20**: 2851–61.
26 Sasaki D, Imaizumi Y, Hasegawa H *et al.* Overexpression of enhancer of zeste homolog 2 with trimethylation of lysine 27 on histone H3 in adult T-cell leukemia/lymphoma as a target for epigenetic therapy. *Haematologica* 2011; **96**: 712–9.
27 Smith MR, Greene WC. Identification of HTLV-I tax trans-activator mutants exhibiting novel transcriptional phenotypes. *Genes Dev* 1990; **4**: 1875–85.
28 Tsuji T, Sheehy N, Gautier VW, Hayakawa H, Sawa H, Hall WW. The nuclear import of the human T lymphotropic virus type I (HTLV-1) tax protein is carrier- and energy-independent. *J Biol Chem* 2007; **282**: 13875–83.
29 Lauth M, Bergström A, Shimokawa T, Toftgård R. Inhibition of GLI-mediated transcription and tumor cell growth by small-molecule antagonists. *Proc Natl Acad Sci USA* 2007; **104**: 8455–60.
30 Blair HJ, Tompson S, Liu YN *et al.* Evc2 is a positive modulator of Hedgehog signalling that interacts with Evc at the cilia membrane and is also found in the nucleus. *BMC Biol* 2011; **9**: 14.
31 Ego T, Ariumi Y, Shimotohno K. The interaction of HTLV-1 Tax with HDAC1 negatively regulates the viral gene expression. *Oncogene* 2002; **21**: 7241–6.
32 Kamoi K, Yamamoto K, Misawa A *et al.* SUV39H1 interacts with HTLV-1 Tax and abrogates Tax transactivation of HTLV-1 LTR. *Retrovirology* 2006; **3**: 5.

Supporting Information

Additional supporting information may be found in the online version of this article:

Fig. S1. HTLV-1 *HBZ* does not affect EVC expression.

Fig. S2. EVC knockdown reduces ATL cell proliferation.

Methods S1. Including: details of clinical samples; and primer sequences used in the present study.